REVIEWS OF TOPICAL PROBLEMS

PACS numbers: **12.10.–g**, 12.60.Jv, **29.20.–c**

Search for supersymmetry with *R*-parity violation at the ATLAS facility

V A Bednyakov, E V Khramov

DOI: https://doi.org/10.3367/UFNe.2021.08.039034

Contents

1. **Introduction** **997**
2. **ATLAS detector** **1000**
3. **Decays into a pair of different leptons** **1002**
4. **Multilepton final states** **1005**
5. **Multijet decays of gluino or squark pairs** **1007**
6. **Multijet events with two identically charged leptons or three leptons** **1011**
7. ***R*-parity violation and third-generation squarks** **1013**
8. **Conclusion** **1017**

References **1017**

Abstract. In 2009–2018, the first and second operation phases (Run 1 and Run 2) of the Large Hadron Collider (LHC) were completed at CERN at proton–proton energies $\sqrt{s} = 7-8$ and 13 TeV. One of the major goals in constructing the LHC was successfully accomplished with the discovery of the Higgs boson, the missing and fundamentally important element of the modern Standard Model of elementary particles. Along with this, a large amount of other unique physical information was obtained. We review the procedure for obtaining new physical results in the search for supersymmetry with R-parity violation at the ATLAS (A Toroidal LHC ApparatuS) facility. A comparison with the results of other, mainly collider, experiments is given.

Keywords: ATLAS, Large Hadron Collider, supersymmetry, *R*-parity violation

1. Introduction

Over the past decades, the Standard Model (SM) of particle physics has proved itself to be an excellent tool to successfully describe and predict the results of experiments in a wide range of phenomena and energies, with amazing accuracy. The long-awaited discovery of the Higgs boson in the ATLAS (A Toroidal LHC ApparatuS) [1] and CMS (Compact Muon Solenoid) [2] experiments at the Large Hadron Collider (LHC) was the definitive triumph of this model.

But, although the SM certainly is an outstanding achievement of the human mind, it still has a number of significant shortcomings. For example, there is no explanation for the mass spectrum and coupling constants of elementary particles within the SM [3, 4], nor is there a candidate for the role of a dark matter particle [5]; the quantum theory of gravity is not in the model, and the role of dark energy is unclear (see, e.g., [6–8]).

For these reasons, the main task of the current stage in the development of elementary particle physics, which underlies the modern-day worldview, is the construction of a new, more general model (theory) of the physical world, one that would at least be free of the noted shortcomings of the SM. In addition to the numerous attempts at a purely theoretical construction of candidates for such a theory (see, e.g., [9–15]), the decisive source of data needed for that purpose is the so-called search for New Physics on all energy scales presently accessible to researchers, i.e., the search for new physical phenomena (particles, interactions, etc.) whose SM description is impossible.

It is known that, in addition to the successful discovery of the Higgs boson, the search for possible manifestations of New Physics was the second major objective of constructing both the unique Large Hadron Collider (LHC) and four, also unique, multipurpose detector complexes: ATLAS, CMS, ALICE (A Large Ion Collider Experiment), and LHCb (Large Hadron Collider beauty experiment).

Unfortunately, the second task turned out to not be as 'simple' as the first one. Despite extensive research programs to seek manifestations of New Physics in experiments at the LHC, including the ATLAS experiment, no signatures of New Physics have been found so far. This makes the search for New Physics even more relevant and intriguing because it, obviously, 'must be around.' Apparently, new ideas and new search methods are needed.

On the other hand, when discovered sooner or later, New Physics will appear as a better theoretical model (compared with the current SM) in which all new phenomena will be properly attributed and explained.

The most attractive approach from this standpoint, in our opinion, is the extension of the SM based on the idea of supersymmetry (SUSY) [16–21]. This idea, in principle,

V A Bednyakov (*), **E V Khramov** (†)
Joint Institute for Nuclear Research,
ul. Joliot-Curie 6, 141980 Dubna, Moscow region, Russian Federation
E-mail: (*) bedny@jinr.ru, (†) khramov@jinr.ru

Received 28 May 2021, revised 26 July 2021
Uspekhi Fizicheskikh Nauk **192** (10) 1065 – 1088 (2022)
Translated by S Alekseev

allows describing all phenomena of both the 'old' and New Physics with a set of parameters, which, even if quite large, is common to all phenomena and underlies the mass spectrum of all particles and all coupling constants; moreover, the coupling constants are unified and a candidate for the role of a particle of galactic dark matter naturally arises, and numerous other benefits follow [22–27].

Supersymmetry implies the existence of supersymmetric partners to all fundamental particles of the SM. Each SM particle and its superpartner have exactly the same quantum numbers except spin, which differs by $\pm 1/2$: if an SM particle is a boson, its superpartner is a fermion, and vice versa. Obviously, this doubles the number of degrees of freedom, which clearly contradicts observations, and hence there must be a mechanism of so-called soft SUSY breaking, which leads to a significant increase in the masses of all superparticles.

The most attractive and currently well-developed mechanism is the so-called Minimal Supersymmetric extension of the Standard Model (MSSM).

A well-known feature of the SM is the presence of two global symmetries, U_{1B} and U_{1L}, corresponding to the conservation of the baryon and lepton numbers, B and L. These symmetries are a consequence of the gauge symmetry of the SM and the minimal set of SM fields.

In the MSSM, the U_{1B} and U_{1L} symmetries are broken, and therefore processes that violate the lepton and baryon numbers are possible. In particular, this means that matter is unstable due to proton decay.

The standard way to deal with this problem is to *artificially* introduce a discrete symmetry called R-parity [28], a multiplicative symmetry defined as

$$R = (-1)^{3B+L+2S}\,, \tag{1}$$

where S, B, and L are the respective spin, baryon, and lepton quantum numbers. It hence follows that all SM particles have a conserved multiplicative quantum number $R = +1$, and all their superpartners have $R = -1$.

The R-parity conservation (RPC) prevents lepton- and baryon-number-violating processes: superpartners can only be produced in pairs, and the lightest SUSY particle is stable. Although R-parity is attractive for a number of reasons, the requirement to preserve it does not have good theoretical grounds. For example, a particular R-parity violation (RPV) can shed light on the problem of the origin of the neutrino mass [29]: in this framework, neutrinos can acquire a supersymmetric mass at the tree level by mixing with gauginos and higgsinos on a weak scale [30–34]. This mechanism, in contrast to the seesaw mechanism, does not affect the physics on large energy scales $M_{\text{int}} \sim \mathcal{O}(10^{12}\text{ GeV})$: it relates the neutrino mass to the electroweak scale, which is accessible for experimental verification.

In a model without RPC, single supersymmetric particles can decay into ordinary particles. Such processes can therefore be studied using conventional particle detectors.

It follows that the MSSM is the minimal extension of the SM that incorporates the idea of supersymmetry. The model is based on the SM gauge group $G_{\text{SM}} = SU(3)_c \times SU(2)_L \times U(1)_Y$ and the minimal content of fundamental fields listed in the table.

Instead of one doublet of Higgs bosons in the SM, the list of superfields includes two doublets of Higgs bosons, $\widehat{H}_1$ and $\widehat{H}_2$, with respective weak hypercharges $Y = -1$ and $+1$. The second Higgs superfield, $\widehat{H}_2$, is needed to construct the SUSY

Table. Complete set of MSSM fields. Rightmost column shows quantum numbers of fields with respect to the $SU(3)_c \times SU(2)_L \times U(1)_Y$ group, i.e., multiplicity with respect to the strong group, the third component of weak isospin T_3, and hypercharge $Y = 2(Q - T_3)$, where Q is the electric charge.

Superfields	Bosons, spin = 0, 1	Fermions, spin = 1/2	Quantum numbers
$\widehat{g}^{(a)}$	$g^{(a)}$ gluons	$\widetilde{g}^{(a)}$ gluinos	(8, 1, 0)
$\widehat{W}^{(k)}$	$W^{(k)}$ W bosons	$\widetilde{W}^{(k)}$ winos	(1, 3, 0)
$\widehat{B}$	B *B* field	$\widetilde{B}$ binos	(1, 1, 0)
$\widehat{L}$	$\widetilde{L} = \begin{pmatrix} \widetilde{\nu}_L \\ \widetilde{e}_L^- \end{pmatrix}$	$L = \begin{pmatrix} \nu_L \\ e_L^- \end{pmatrix}$	(1, 2, −1)
$\widehat{E}^C$	$\widetilde{E}^C = (\widetilde{e}_R)^*$ sleptons	$E^C = (e_R^-)^C$ leptons	(1, 1, 2)
$\widehat{Q}$	$\widetilde{Q} = \begin{pmatrix} \widetilde{u}_L \\ \widetilde{d}_L \end{pmatrix}$	$Q = \begin{pmatrix} u_L \\ d_L \end{pmatrix}$	$\left(3, 2, \frac{1}{3}\right)$
$\widehat{U}^C$	$\widetilde{U}^C = (\widetilde{u}_R)^*$	$U^C = (u_R)^C$	$\left(3, 1, -\frac{4}{3}\right)$
$\widehat{D}^C$	$\widetilde{D}^C = (\widetilde{d}_R)^*$ squarks	$D^C = (d_R)^C$ quarks	$\left(3, 1, \frac{2}{3}\right)$
$\widehat{H}_1$	$H_1 = \begin{pmatrix} H_1^0 \\ H_1^- \end{pmatrix}$	$\widetilde{H}_1 = \begin{pmatrix} \widetilde{H}_1^0 \\ \widetilde{H}_1^- \end{pmatrix}$	(1, 2, −1)
$\widehat{H}_2$	$H_2 = \begin{pmatrix} H_2^+ \\ H_2^0 \end{pmatrix}$ Higgs bosons	$\widetilde{H}_2 = \begin{pmatrix} \widetilde{H}_2^+ \\ \widetilde{H}_2^0 \end{pmatrix}$ Higgsinos	(1, 2, 1)

Yukawa coupling $\widehat{H}_2\widehat{Q}\widehat{U}^C$, which provides the u-quark masses after electroweak symmetry breaking.

The general gauge-invariant form of a renormalizable superpotential is

$$W = W_{\not R} + W_R\,. \tag{2}$$

Its parity-preserving part has the standard MSSM form

$$W = \varepsilon_{ab}\Big[h_{ij}^E \widehat{H}_1^a \widehat{L}_i^b \widehat{E}_j^C + h_{ij}^D \widehat{H}_1^a \widehat{Q}_i^b \widehat{D}_j^C - h_{ij}^U \widehat{H}_2^a \widehat{Q}_i^b \widehat{U}_j^C - \mu \widehat{H}_1^a \widehat{H}_2^b\Big]\,, \tag{3}$$

where $i, j = 1, 2, 3$ are generation indices and $a, b = 1, 2$ are indices of the $SU(2)_L$ group. The totally antisymmetric tensor ε is defined as $\varepsilon_{12} = -\varepsilon_{21} = 1$. The hats above symbols denote superfields.

The R-parity-violating part of superpotential (2) is usually written as [30, 35–37]

$$W_R = \varepsilon_{ab}\left[\frac{1}{2}\lambda_{ijk}\widehat{L}_i^a \widehat{L}_j^b \widehat{E}_k^C + \lambda'_{ijk}\widehat{L}_i^a \widehat{Q}_j^b \widehat{D}_k^C - \mu_j \widehat{L}_j^a \widehat{H}_2^b\right] + \frac{1}{2}\lambda''_{ijk}\widehat{U}_i^C \widehat{D}_j^C \widehat{D}_k^C\,. \tag{4}$$

The coupling constants λ (λ'') are antisymmetric in the first (last) two indices, as required by SU(2) and SU(3) invariances.

As we have noted, due to the observed mass spectrum of elementary particles, supersymmetry can have some realistic phenomenology only when it is explicitly broken at low energies, which manifests itself in the different masses of the superpartners.

SUSY can be broken in the so-called soft way, so as to maintain the important ultraviolet property of SUSY, which is the absence of quadratic divergences. We recall that this SUSY property allows solving the hierarchy problem, which was one of the main reasons for invoking the idea of supersymmetry.

The MSSM Lagrangian with soft SUSY breaking has the form

$$\mathcal{L}_{\text{soft}} = -V^{\text{soft}} - V_R^{\text{soft}} + \mathcal{L}_{\text{GM}}^{\text{soft}}\,, \tag{5}$$

where the RPC (V^{soft}) and RPV (V_R^{soft}) terms of the scalar potential are

$$\begin{aligned} V^{\text{soft}} &= (M_Q^2)_{ij}\widetilde{Q}_i^{a*}\widetilde{Q}_j^a + (M_U^2)_{ij}\,\widetilde{u}_{\text{R}i}^*\widetilde{u}_{\text{R}j} + (M_D^2)_{ij}\,\widetilde{d}_{\text{R}i}^*\widetilde{d}_{\text{R}j} \\ &+ (M_L^2)_{ij}\widetilde{L}_i^{a*}\widetilde{L}_j^a + (M_E^2)_{ij}\,\widetilde{e}_{\text{R}i}^*\widetilde{e}_{\text{R}j} + m_{H_1}^2 H_1^{a*}H_1^a \\ &+ m_{H_2}^2 H_2^{a*}H_2^a + \varepsilon_{ab}\big[A_U^{ij}h_{ij}^U\widetilde{Q}_i^a\widetilde{u}_{\text{R}j}^*H_2^b + A_D^{ij}h_{ij}^D\widetilde{Q}_i^b\widetilde{d}_{\text{R}j}^*H_1^a \\ &+ A_E^{ij}h_{ij}^E\widetilde{L}_i^b\,\widetilde{e}_{\text{R}j}^*H_1^a - B\mu H_1^aH_2^b + \text{h.c.}\big]\,, \end{aligned} \tag{6}$$

$$\begin{aligned} V_R^{\text{soft}} &= \varepsilon_{ab}\big[\Lambda_{ijk}\widetilde{L}_i^a\widetilde{L}_j^b\,\widetilde{e}_{\text{R}k}^* + \Lambda'_{ijk}\widetilde{L}_i^a\widetilde{Q}_j^b\widetilde{d}_{\text{R}k}^* + \widetilde{\mu}_{2j}^2\widetilde{L}_j^aH_2^b\big] \\ &+ \widetilde{\mu}_{1j}^2\widetilde{L}_j^aH_1^{a*} + \Lambda''_{ijk}\widetilde{u}_{\text{R}i}^*\widetilde{d}_{\text{R}j}^*\widetilde{d}_{\text{R}k}^* + \text{h.c.} \end{aligned} \tag{7}$$

The 'soft' mass term for the superpartners of gauge bosons (gauginos) has the form

$$\mathcal{L}_{\text{GM}}^{\text{soft}} = -\frac{1}{2}\big[M_1\widetilde{B}\widetilde{B} + M_2\widetilde{W}^k\widetilde{W}^k + M_3\widetilde{g}^a\widetilde{g}^a\big] - \text{h.c.} \tag{8}$$

The tildes denote superpartners of the SM fields. We note that, for the gluino $\tilde{g}$, the 'soft' mass M_3 coincides in this case with its physical mass, denoted as $m_{\tilde{g}} = M_3$ in what follows. At the same time, the 'soft' masses $M_{1,2}$ are not the physical masses of the $\widetilde{W}$ and $\widetilde{B}$ fields, because they are in general mixed with each other and with the higgsino and neutrino masses. The mass eigenstates of these objects are determined below by diagonalizing the corresponding total mass states of a 7×7 matrix.

A characteristic feature of SUSY extensions of the SM is the presence of renormalizable operators that violate the conservation laws for the lepton, L, and baryon, B, numbers. These operators, which are present in formulas (4) and (7), also violate the R-parity. In the SM, L- and B-violating renormalizable operators are forbidden by gauge invariance and the field content. In supersymmetric extensions of the SM, this limitation is lifted due to a wider spectrum of physical fields (see the table).

Overall, the SUSY model characterized by superpotential (2) and soft supersymmetry breaking condition (5), which does not preserve R-parity, is called the 'MSSM with broken R-parity' proper. It contains 135 independent R-violating parameters: 9 bilinear mass parameters μ_j, $\tilde{\mu}_{1j}$, and $\tilde{\mu}_{2j}$, 9 trilinear parameters of the λ type, 27 of the λ' type, 9 of the λ'' type, and 3×27 of the Λ, Λ', and Λ'' types.

It is generally accepted that the simultaneous presence in expressions (4) and (7) of terms that violate the lepton and baryon numbers (unless, of course, these terms are guaranteed to be very small for some reason) gives rise to an observable proton decay probability that is too high. Therefore, it is usually assumed that, in any phenomenologically acceptable SUSY model, either lepton-number-violating or baryon-number-violating terms alone can be present. If we assume *a priori* that the R-parity is strictly conserved, then it is obvious that all 'inconvenient' terms vanish; the corresponding SUSY model is known as the MSSM. We note, however, that this does not seem to be sufficiently well substantiated in the context of this review.

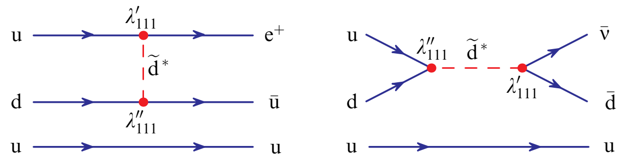

Figure 1. (Color online.) Example of proton decay due to R-parity violation.

To complete the picture, we present several arguments in favor of the models with broken R-parity and briefly discuss other variants of discrete symmetries.

As we have noted, the terms that violate the conservation law of the lepton and baryon numbers in both the superpotential W_R, Eqn (4), and the scalar potential V_R, Eqn (7), which softly violates SUSY, may well lead to an experimentally unacceptable proton decay rate (Fig. 1). This can occur due to products of the coupling constants that break lepton and baryon symmetries, e.g., in the form $\lambda''\lambda'$, $\lambda''\lambda$, and $\lambda''\mu_i$. At present, the lower bound for the proton lifetime is $\tau > 10^{31} - 10^{33}$ years [38], and the proton decay width for the channels shown in Fig. 1 can be evaluated as

$$\begin{aligned} \Gamma(\text{p} \to \text{e}^+\pi^0) &\approx \frac{|\lambda'_{11k}|^2|\lambda''_{11k}|^2}{16\pi^2 m_{\tilde{\text{d}}_k}^4}\,M_{\text{proton}}^5\,, \\ \Gamma(\text{p} \to \bar{\nu}\pi^+) &\approx \frac{|\lambda'_{i1k}|^2|\lambda''_{11k}|^2}{16\pi^2 m_{\tilde{\text{d}}_k}^4}\,M_{\text{proton}}^5\,, \\ \Gamma(\text{p} \to \nu\pi^+) &\approx \frac{|\lambda'_{i1k}|^2|\lambda''_{11k}|^2}{16\pi^2 m_{\tilde{\text{d}}_k}^4}\left(\frac{m_{\text{d}_k}}{m_{\tilde{\text{d}}_k}}\right)^2 M_{\text{proton}}^5\,. \end{aligned}$$

For example, with the lifetime bounded below as $\tau > 10^{34}$ years for the proton decay channel $\text{p} \to \text{e}\pi$ [38], we obtain the following bounds for the products of coupling constants of the $\text{p} \to \text{e}^+\pi^0/\bar{\nu}\pi^+$ and $\text{p} \to \nu\pi^+$ decays:

$$\begin{aligned} |\lambda'_{i1k}\lambda''_{11k}| &\lesssim 2 \times 10^{-28}\left(\frac{m_{\tilde{\text{d}}_k}}{M_{\text{W}}}\right)^2, \\ |\lambda'_{ik1}\lambda''_{11k}| &\lesssim 2 \times 10^{-26}\left(\frac{m_{\tilde{\text{d}}_k}}{M_{\text{W}}}\right)^3. \end{aligned}$$

It is clear that these products of coupling constants must be very small in order to agree with the experimental bounds on the proton lifetime, and it is therefore more natural to assume that they are plainly forbidden. This can be achieved by requiring a certain kind of symmetry. In 1987, Farrar and Fayet [28] proposed a discrete Z_2 symmetry for this purpose, which was called the R-parity. The action of the corresponding operator on the superpotential and on the soft SUSY-violating potential was defined as

$$\begin{aligned} \hat{R}W &= W\,, \qquad \hat{R}W_R = -W_R\,, \\ \hat{R}V &= V\,, \qquad \hat{R}V_R = -V_R\,. \end{aligned} \tag{9}$$

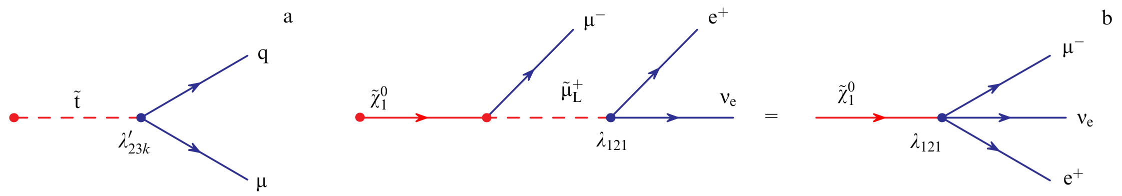

Figure 2. (Color online.) Feynman diagrams for (a) RPV decay of a $\tilde{t}$ squark into a quark and a muon for $\lambda'_{23k} \neq 0$ and (b) three-lepton decay $\tilde{\chi}_1^0$ for $\lambda_{121} \neq 0$.

Let us recall that the quantum number $R = (-1)^{3B+L+2S}$ in (1) is $+1$ for ordinary SM particles and -1 for their superpartners. Imposed *ad hoc* on the MSSM, this symmetry forbids all RPV couplings and automatically guarantees that B and L numbers are preserved at the level of renormalizable operators.

Recall that various discrete symmetries have no deep theoretical justification, except the proton stability requirement. We cannot say *a priori* which of these symmetries is preferable. The answer to a question of this kind should apparently be sought in the framework of some more fundamental theory, such as the Grand Unified Theories (GUTs) [30, 39–41], models with extra spatial dimensions [42], or string theory [14, 43, 44]. At present, there is no decisive argument in favor of a particular SUSY model that preserves or violates the R-parity. Therefore, when searching for SUSY, it is necessary to take both of the possibilities mentioned above into account, with their totally different phenomenological consequences.

Indeed, RPV leads to the removal of restrictions on processes violating the baryon and lepton number conservation. Production of single supersymmetric particles becomes possible. When R-parity is preserved, supersymmetric particles can be created and decay only in pairs. The lightest SUSY particle (LSP) is stable: it cannot decay into SM particles.

In addition to the proton decay already mentioned (see Fig. 1), other exotic processes become possible, such as the decay $\tau^- \to e^- + \nu_\mu + \bar{\nu}_e$. Neutrinos can acquire Majorana masses by mixing with gauginos and higgsinos, as well as through loop diagrams.

The neutralino is no longer necessarily an LSP, this role being taken over by other superparticles,

$$\mathrm{LSP} \in \{\chi_1^0, \chi_1^\pm, \tilde{g}, \tilde{q}, \tilde{t}, \tilde{\ell}, \tilde{\nu}\},$$

which is potentially accompanied by a rather specific phenomenology. An unstable LSP can decay both inside and outside the detector, for example, via $\chi \to \mu\, u\, \bar{d}$ or 'invisibly' into three neutrinos: $\chi \to \nu\,\nu\,\tilde{\nu}$. Because the LSP is unstable, it is no longer preferable for the role of a galactic dark matter particle (the possibility and necessity of detecting it in astrophysical, accelerator, and underground experiments is discussed in [45, 46]). However, we note that, with a sufficiently long lifetime of an unstable LSP, it can still serve as a candidate for the role of a dark matter particle if

$$\tau_\chi^0 \gg t_0\,, \tag{10}$$

where τ_χ^0 is the LSP lifetime and t_0 is the age of the Universe. But, in the framework of accelerator experiments, the signature of events should be similar to the signature of a stable LSP. The LSP can then only decay into SM particles.

Nonzero values of the coupling constants λ in formula (4) lead, for example, to $\tilde{t}$-squark decay into a q quark and a muon if $\lambda'_{23k} \neq 0$ (here, the subscript 2 corresponds to the muon, the subscript 3, to the $\tilde{t}$ squark, and $k = 1, 2, 3$ means that the q quark can be from any generation) or successive neutralino decay: first into an electron (muon) and a selectron (smuon) with RPC, after which the selectron (smuon) decays into a neutrino and an electron (muon) due to the RPV coupling constant $\lambda_{121} \neq 0$, as shown in Fig. 2.

One of the key consequences of RPC manifested in the production of SUSY particles at high energies is the possibility of observing a large missing momentum (E_T^{miss}) due to nondecaying and unregistered LSPs. However, to date, no significant indications that supersymmetry exists have been found in any channel with the expected RPC signature in experiments at the LHC. In fact, all observed events with a sufficiently large E_T^{miss} were satisfactorily described in terms of the SM. This adds interest to signatures with RPV and without E_T^{miss} in particular.

In this review, we describe the development of methods for the analysis of experimental data to search for SUSY in scenarios with RPV in various possible processes of production and decay of SUSY particles at the ATLAS facility. In addition, a comparison is made with the results obtained at the CMS installation and calculated on the basis of other experimental data.

We deliberately omit the description of methods for estimating systematic errors and methods for reconstructing physical objects (hadron jets, electrons, muons, etc.) and focus on methods for selecting events and estimating contributions from background processes.

Previously, similar searches were also carried out in experiments at the Tevatron accelerator at the Fermi National Accelerator Laboratory (USA) [47–57]. A theoretical analysis of the prospects for the search and study of SUSY with violated R-parity at the LHC can be found, e.g., in [58–61].

To conclude the introduction, we note that both the results discussed here and numerous other important results were provided by the stable operation of the ATLAS multipurpose detector, which is currently being maintained and operated by institutions from 40 countries from around the world.

2. ATLAS detector

The LHC is a proton–proton collider with a maximum center-of-mass energy of 14 TeV and a design luminosity of 10^{34} cm^{-2} s^{-1}, which was already exceeded by a factor of 1.5 in 2016 and reached 2×10^{34} cm^{-2} s^{-1} in 2018 [62]. At the design luminosity, the beams are expected to cross every 25 ns, with an average of 23 interactions in each such intersection (the average number of interactions per intersection reached 60 in 2018). The accelerator, with a length of 27 km, is located underground at a depth of 50 to 175 m in a tunnel 3.8 m in

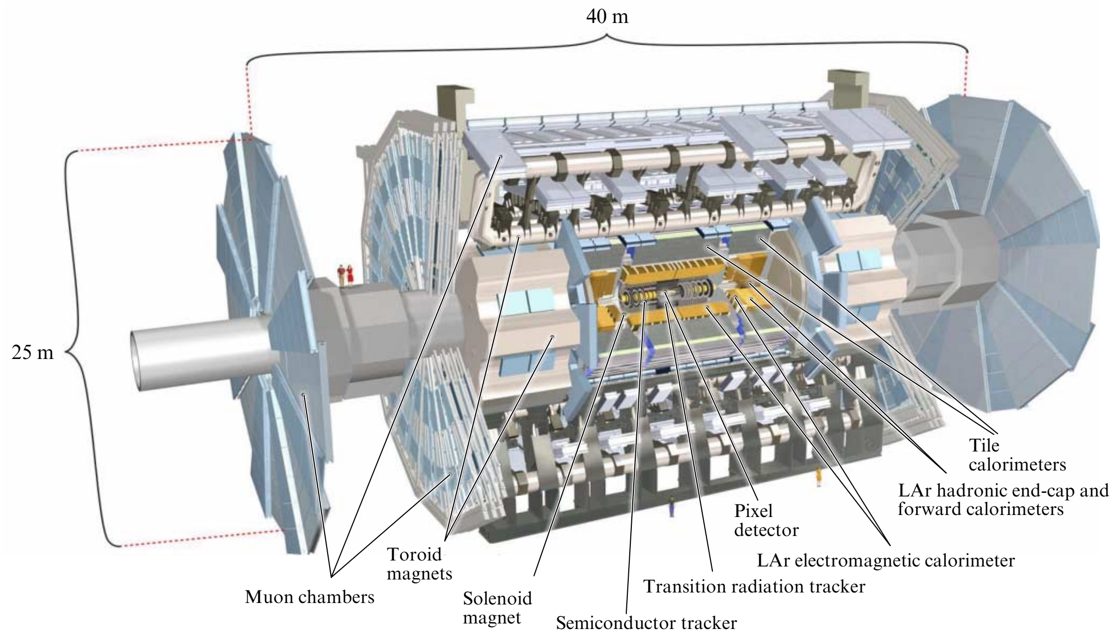

Figure 3. (Color online.) ATLAS installation.

diameter. A complete beam revolution at the LHC was first achieved on September 10, 2008 at a beam energy of 450 GeV.

The LHC has huge potential for the search for New Physics and for precision measurements of the already known SM parameters. The LHC is also called the top-quark factory, because, even at a low accelerator luminosity (10^{33} cm^{-2} s^{-1}), about 8 million top–antitop quark pairs are expected. The unprecedentedly high collision energy of proton beams allows carrying out research in the energy range up to several TeV. It is assumed that the data obtained at the four experimental LHC facilities, ATLAS, CMS, ALICE, and LHCb, will help in answering many questions currently facing modern physics.

The ATLAS and CMS experiments have physics research programs that are similar in many respects. Some of them are to confirm or improve SM measurements, but one of the most important tasks to be explored in the ATLAS experiment is to explain the mechanism of electroweak symmetry breaking. One such mechanism is the Higgs mechanism, which assumes the existence of the Higgs boson. In addition, there are other models of electroweak symmetry breaking, such as the technicolor model. Other major programs at ATLAS include the study of top-quark physics, supersymmetry, B-physics, heavy-ion physics, and exotic physics.

The ATLAS installation [63] at the LHC is a multipurpose elementary particle detector of a cylindrical shape with interaction point coverage reaching the solid angle of 4π (Fig. 3).[1] It consists of an inner detector (ID) surrounded by a superconducting solenoid, electromagnetic and hadron calorimeters, and a muon spectrometer built in to a system of three toroidal magnets.

The ID, placed in a magnetic field of 2 T, is designed to determine the tracks of charged particles in the range $|\eta| < 2.5$. The silicon detector, which has a high degree of granularity, covers the vertex reconstruction region, and four signals from the particle track were usually recorded in it: the first signal was typically in the so-called B-layer [64–66], located immediately behind the beam channel at a radius of 33 mm from the proton collision line. Three more concentric layers of the pixel detector are located at radii of 50.5 mm, 88.5 mm, and 122.5 mm in front of the first active layer of the semiconductor track detector located at radius $r = 299$ mm. A semiconductor detector based on silicon microstrips records eight signals per track on average. The silicon detector layers were supplemented by a transition radiation track system consisting of drift chambers in the form of long thin tubes, which increases the pseudorapidity coverage region for track reconstruction to $|\eta| < 2.0$.

In the pseudorapidity central region, particle energy is measured using a highly granular liquid argon electromagnetic calorimeter with a lead absorber and a scintillation hadronic calorimeter with a steel absorber ($|\eta| < 1.475$ and $|\eta| < 1.7$, respectively). For the pseudorapidity range up to $|\eta| < 4.9$, liquid argon electromagnetic and hadron calorimeters are used.

The muon spectrometer surrounding the calorimeter system is built in to three large superconducting toroidal magnets, each with eight coils. The magnetic field of toroidal magnets varies from 2 to 6 T per meter in almost the entire volume of the detector. The muon spectrometer is a system of precision tracking cameras and a fast trigger system. Three layers of drift tube chambers provide high-precision measurements of the muon track curvature in the range $|\eta| < 2$, while two layers of drift tube chambers and one layer of cathode-strip chambers provide measurements in the range $|\eta| < 2.7$. Planar resistive chambers serve to trigger muons for

[1] In the ATLAS experiment, a right-handed coordinate system is used with the origin at the nominal interaction point at the center of the detector and with the z-axis directed along the beam axis. The x-axis is directed from the point of interaction to the center of the LHC ring, and the z-axis is directed vertically upward. Cylindrical coordinates (r, ϕ) are used in the transverse plane: azimuthal angle ϕ lies in the plane perpendicular to the z-axis. The pseudorapidity is defined in terms of polar angle θ as $\eta = -\ln\tan(\theta/2)$. The angular distance is measured in units of $R = \left[(\Delta\eta)^2 + (\Delta\phi)^2\right]^{1/2}$.

$|\eta| < 1.05$; in the range $|\eta| < 2.4$, thin-gap gas chambers are used for this purpose.

Events of interest are selected for recording using an electronically-based first-level trigger system; after that, events are selected using high-level software trigger algorithms [67]. The first level trigger makes decisions at a frequency similar to the proton bunch crossing frequency, 40 MHz, and allows storing selected events at a frequency of 100 kHz, which are subsequently recorded after the selection of high-level triggers at a frequency of 1 kHz.

3. Decays into a pair of different leptons

The SUSY model with lepton number violation in the processes of direct production of a single sneutrino followed by decay into an electron–muon pair ($pp \to \tilde{\nu} \to e^{\pm}\mu^{\mp}$) (Fig. 4) was first considered at the LHC by the ATLAS collaboration.

A search was made for the $e^{\pm}\mu^{\mp}$ pair in the final state at the proton collision energy $\sqrt{s} = 7$ TeV using data corresponding to the integrated luminosity 35 pb^{-1} [68]. The results obtained were soon substantially improved using data corresponding to the integrated luminosity 1 fb^{-1} [69]. A significant increase in the amount of data allowed selecting events more rigorously by increasing the lower bound for the transverse momentum of leptons, $p_T = (p_x^2 + p_y^2)^{1/2}$, from 20 to 25 GeV, and also by increasing the lepton isolation radius from $\Delta R = 0.2$ to 0.4 (this determines the size of the cone in which the total energy should not exceed the threshold value).

The SM processes considered the background were the production of pairs of vector bosons (WW, WZ, and ZZ), $Z/\gamma^* \to \tau\tau$, and of $t\bar{t}$ pairs, and single t-quark production, which were accompanied by the presence of $e^{\pm}\mu^{\mp}$ pairs in the final state. Also considered the background were the processes of the formation of $W/Z + \gamma$ and W/Z + jets, and multi-jet processes in which a photon or one or two hadron jets were erroneously reconstructed as a lepton. All background processes were simulated using Monte Carlo event generators, were reconstructed using a program based on GEANT4 [72], and were normalized to the corresponding integrated luminosity.

As can be seen in Fig. 5, the observed upper bounds for the cross section of the production of a tau-slepton with its decay into an $e^{\pm}\mu^{\mp}$ pair were improved by almost an order of magnitude, and the bound for the considered theoretical models was improved almost two-fold.

Also, at $\sqrt{s} = 7$ TeV and the integrated luminosity 2.1 fb^{-1}, the ATLAS collaboration tested the lepton flavor violating (LFV) model of $e^{\pm}\mu^{\mp}$ production via the t-channel exchange of a $\tilde{t}$ squark in $q\bar{q}$-interaction, as shown in Fig. 6. Here, as in Fig. 4, two RPV vertices are present.

The contribution from background processes with erroneous reconstruction of one or two hadronic jets or a nonisolated lepton as an isolated lepton (W/Z + jets and

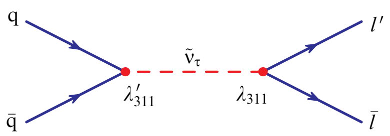

Figure 4. (Color online.) Diagram of RPV production of a tau slepton and its RPV decay into a pair of charged leptons with different lepton numbers.

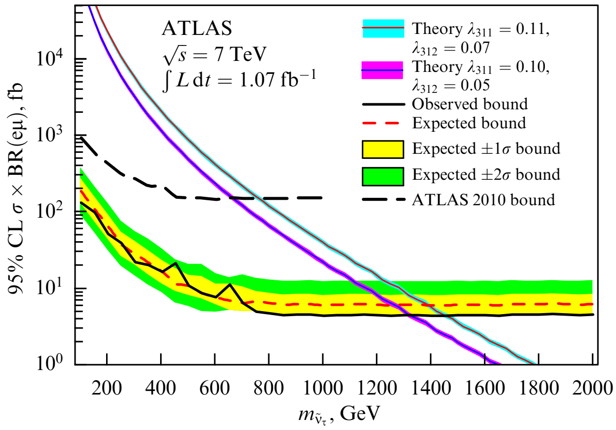

Figure 5. (Color online.) Observable upper bounds for the cross section for the production of a tau slepton with its decay into a $e^{\pm}\mu^{\mp}$ pair, $\sigma(pp \to \tilde{\nu}_\tau) \times BR(\tilde{\nu}_\tau \to e\mu)$, at a 95% confidence level as a function of the tau-slepton mass $m_{\tilde{\nu}_\tau}$, at $\sqrt{s} = 7$ TeV. Expected bounds are shown with the total error taken into account within ± 1 and ± 2 standard deviations. Previously published results [68] and theoretical cross sections of the process [70, 71] calculated in the NLO (next-to-leading order) [69] are also presented.

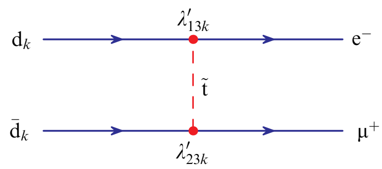

Figure 6. (Color online.) Feynman diagram for the RPV $e^{\pm}\mu^{\mp}$-production process via $\tilde{t}$-squark t-channel exchange in the $q\bar{q}$ interaction with nonzero constants λ'_{13k} and λ'_{23k} [73].

multijet processes), in contrast to the corresponding contribution in the previous analysis [68, 69], was determined by a matrix method using data [73]. The essence of this method is to 're-weigh' events with less stringent criteria for lepton isolation reconstruction so as to include the probability that a lepton present in the event originated from a background process. The weights are obtained by solving an equation involving a 4×4 matrix made of the probabilities that a signal or background lepton that passed the soft selection criteria also passes the standard selection criteria depending on its p_T.

As a result, a bound for the $pp \to e\mu X$ process cross section was established as a function of the $\tilde{t}$-squark mass. As can be seen in Fig. 7a, the upper bound for the process cross section was 170 fb at $m_{\tilde{t}} = 95$ GeV and 30 fb at $m_{\tilde{t}} =$ 1000 GeV.

In addition, these data were recalculated as a combination of the corresponding squares of the RPV coupling constants, taken with the weights given by the proton structure factors,

$$f_{d\bar{d}} |\lambda'_{131}\lambda'_{231}|^2 + f_{s\bar{s}} |\lambda'_{132}\lambda'_{232}|^2 .$$

As shown in Fig. 7b, it was possible to exclude the near-diagonal region for this combination in the range of 6×10^{-4}–0.3 for $100 < m_{\tilde{t}} < 1000$ GeV at a 95% confidence level.

A 'competing' source of nonaccelerator bounds on similar RPV constants is, for example, the recently measured new bound for the $\mu \to e\gamma$ process. For $BR(\mu \to e\gamma) < 4.2 \times 10^{-13}$ [38], the following upper bounds can be obtained for the

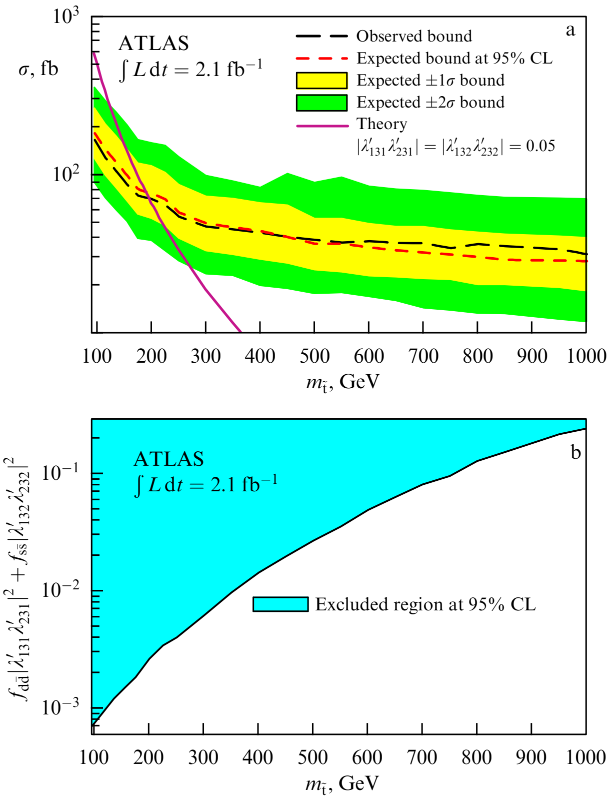

Figure 7. (Color online.) (a) Observable upper bounds for the cross section of the pp $\to$ eμX process via a $\tilde{t}$-squark t-channel exchange as a function of $m_{\tilde{t}}$ at a 95% confidence level. Expected bounds are shown with the total error taken into account within ± 1 and ± 2 standard deviations. (b) Range of the combination $f_{d\bar{d}}\,|\lambda'_{131}\lambda'_{231}|^2 + f_{s\bar{s}}\,|\lambda'_{132}\lambda'_{232}|^2$ of squared RPV coupling constants excluded at a 95% confidence level (above the curve) as a function of $m_{\tilde{t}}$ [73].

sfermion mass $m_{\tilde{f}} = 100$ GeV ($m_{\tilde{f}} = 1$ TeV) [74, 75]:

$$|\lambda_{1k1}\lambda_{1k2}| = |\lambda_{231}\lambda_{232}| < 1.0\times10^{-5}\ (< 1.0\times10^{-3})\,,$$
$$|\lambda_{23k}\lambda_{13k}| < 2.0\times10^{-5}\ (< 2.0\times10^{-3})\,,$$
$$|\lambda'_{21k}\lambda_{11k}| = |\lambda'_{22k}\lambda_{12k}| < 2.7\times10^{-5}\ (2.7\times10^{-3})\,,$$
$$|\lambda'_{23k}\lambda_{13k}| < 5\times10^{-4}\ (< 3.5\times10^{-3})\,.$$

At first glance, this example seems to suggest that these nonaccelerator constraints are generally more stringent than the above collider constraints. But, somewhat anticipating the material to follow, we note that such a direct comparison of noncollider and collider constraints (on the products of RPV constants) is extremely difficult and not very informative due to the significant difference both in the assumptions made in the analysis of these data and in the 'systematics,' goals, and setup of accelerator and nonaccelerator experiments [60].

A natural development of this search for RPV SUSY was the addition of the remaining two possible lepton channels to the $e^\pm\mu^\mp$ decay channel considered above:

$$pp \to \tilde{\nu}_\tau \to e^\pm\mu^\mp \quad\text{and}\quad \tilde{\nu}_\tau \to e^\pm\tau^\mp \quad\text{and}\quad \tilde{\nu}_\tau \to \mu^\pm\tau^\mp\,.$$

In this case, the identification of the tau lepton in the final state was carried out only by the hadronic channels of its decay, with the branching ratio BR($\tau \to$ hadrons) > 50%.

In accordance with the SM, τ-lepton decay involves only the ν_τ neutrino, and therefore the entire transverse momentum missing in the event, equal (with the reversed sign) to the vector sum of the transverse momenta of all reconstructed objects (electrons, muons, tauons, photons, and hadronic jets), was assigned to this ν_τ neutrino, and the transverse momentum of the reconstructed τ lepton was vector-corrected by E_T^{miss}.

By analogy with the transverse momentum in selecting an electron and a muon, the transverse momentum of the τ lepton had to exceed 25 GeV. In addition, the contribution from W + jet and multijet processes was determined using data. The W + jets process modeled by the Monte Carlo method was normalized to the data in the kinematic region with an additional criterion, $E_T^{miss} > 30$ GeV, where this process becomes dominant. The contribution of multijet processes is, in turn, determined in the range where two leptons with the same electric charge are selected under the assumption that the probability of reconstructing the hadron jet as a charged lepton is independent of the sign of this charge. With such a selection of events, data were processed for $\sqrt{s} = 7$ and 8 TeV and the respective integrated luminosities of 4.6 and 20.3 fb^{-1} [76, 77].

A significant increase in the data statistics allowed improving the observed upper bounds of the tau-slepton production cross section in the $e^\pm\mu^\mp$ decay channel (Fig. 8a) by an order of magnitude, while at the same time the measured upper bounds for channels with tau leptons (Fig. 8b, c) are slightly worse than those for $e^\pm\mu^\mp$ due to the lower efficiency of tau lepton reconstruction.

In addition, bounds were set for the coupling constant λ'_{311} depending on the tau-sneutrino mass under various assumptions about the value of the coupling constant λ_{i3k} for eμ, eτ, and μτ at a 95% confidence level (see respective Figs 9a, b, c).

A version of this analysis carried out at energy $\sqrt{s} =$ 13 TeV and the data collected in 2015 with the integrated luminosity of 3.2 fb^{-1} [78] are worth noting. For SM processes, the cross section at $\sqrt{s} = 13$ TeV is more than twice that at $\sqrt{s} = 8$ TeV, and the ratio of the cross sections for SUSY processes with such an increase in energy is greater than five.

In addition, an increase in the data statistics and the kinematics of events allowed increasing the lower bounds for transverse momenta to 65 GeV for electrons and muons and to 40 GeV for tauons, which naturally led to a noticeable increase in the sensitivity of the analysis.

As can be seen from Fig. 10, the measured upper bounds of the cross section for tau-slepton production followed by the decay into $e^\pm\mu^\mp$, $e^\pm\tau^\mp$, and $\mu^\pm\tau^\mp$ pairs are three orders of magnitude higher than the upper bounds obtained previously with the data at $\sqrt{s} = 8$ TeV [76].

Looking somewhat unusual compared to the foregoing was an analysis by the ATLAS collaboration, where they considered the hypothesis of a long-lived neutralino $\tilde{\chi}_1^0$ with a lifetime corresponding to $c\tau = 10-1000$ mm but still decaying into a pair of leptons and neutrinos. It was assumed that such a neutralino is produced during the production of a squark–antisquark pair in a pp collision at $\sqrt{s} = 13$ TeV and the corresponding integrated luminosity of 32.8 fb^{-1} [79]. In other words, it was believed that the RPC process of neutralino production occurs first, followed by the RPV process of its decay:

$$pp \to \tilde{q} + \tilde{q}\,, \quad\text{then}\quad \tilde{q} \to q + \tilde{\chi}_1^0 \quad\text{and finally}$$
$$\tilde{\chi}_1^0 \to e^\pm e^\mp \nu \quad\text{or}\quad \tilde{\chi}_1^0 \to e^\pm\mu^\mp\nu \quad\text{and}\quad \tilde{\chi}_1^0 \to \mu^\pm\mu^\mp\nu\,.$$

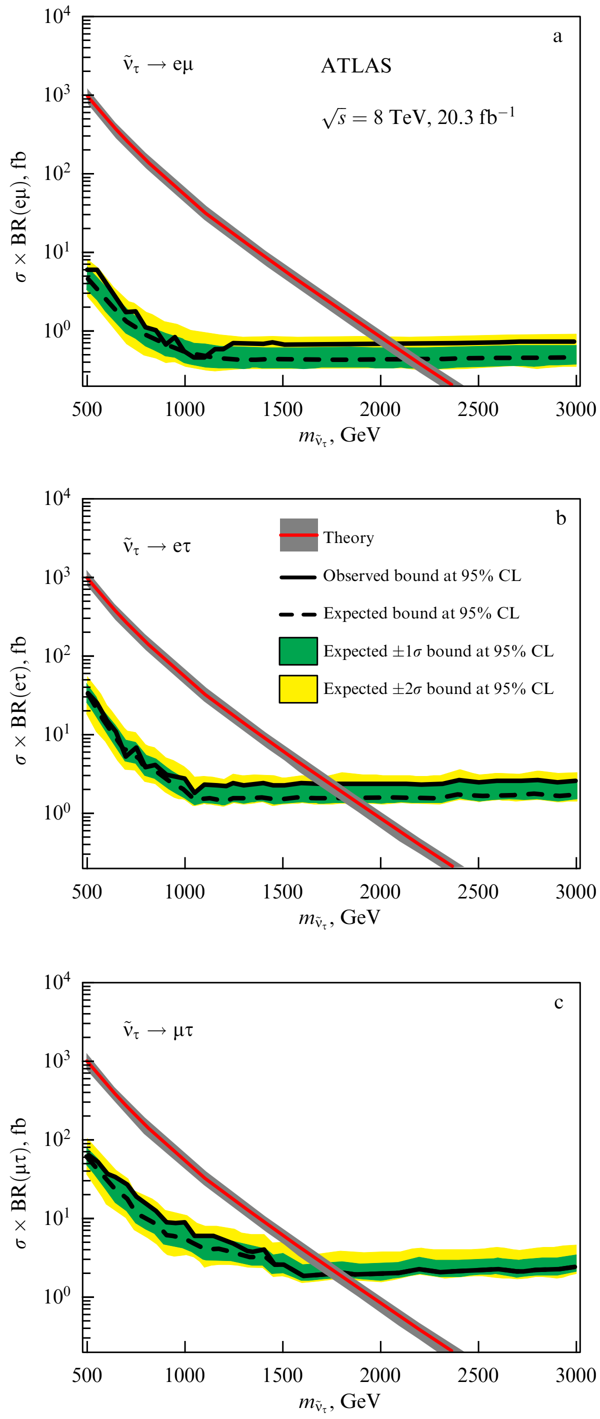

Figure 8. (Color online.) Observed upper bounds for the tau-slepton production cross section in (a) $e^{\pm}\mu^{\mp}$, (b) $e^{\pm}\tau^{\mp}$, and (c) $\mu^{\pm}\tau^{\mp}$ pair decay channels, $\sigma(pp \to \tilde{\nu}_\tau) \times \mathrm{BR}(\tilde{\nu}_\tau \to e\mu/e\tau/\mu\tau)$ at a 95% confidence level as a function of tau-slepton mass $m_{\tilde{\nu}_\tau}$ at $\sqrt{s} = 8$ TeV. Expected bounds are shown with the total error taken into account within ± 1 and ± 2 standard deviations. Theoretical cross sections of the process [70, 71] with total errors [76] are also given.

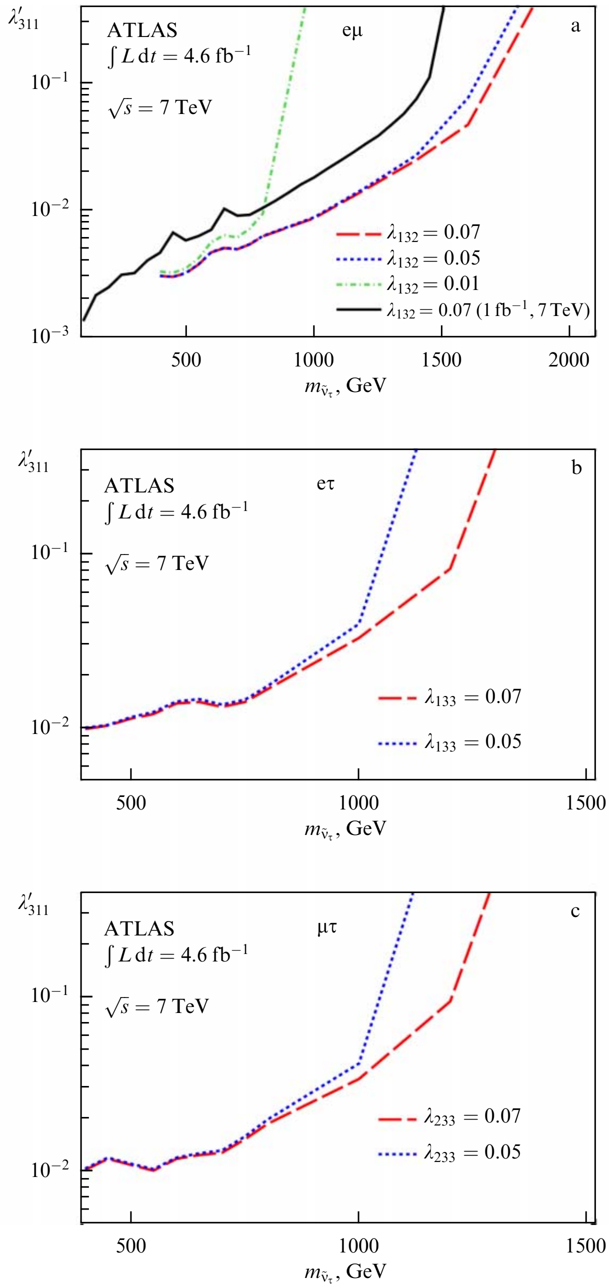

Figure 9. (Color online.) Observed upper bounds for coupling constant λ'_{311} as functions of the tau-sneutrino mass for various assumptions about the value of coupling constant λ_{i3k} for (a) eμ, (b) eτ, and (c) μτ at a 95% confidence level [77]. Also shown are bounds obtained in the previous analysis for integrated luminosity of 1 fb^{-1} and $\sqrt{s} = 7$ TeV [69] for the eμ channel.

The decay channels of both squarks are identical, and the neutralino decay channels are shared equally among the neutralinos, 33% per channel.

The sought events were reconstructed from the secondary vertex, which had to be at least 2 mm away from the primary vertex of the pp interaction in the plane perpendicular to the beam axis, but not farther than 3 m. Also, the invariant mass of all tracks

$$m_{\mathrm{vtx}}^2 = \left[\sum_i^{\mathrm{track}} E_i\right]^2 - \left[\sum_i^{\mathrm{track}} \mathbf{p}_i\right]^2$$

associated with this vertex must be greater than 12 GeV. With this event selection, the main background is given by events from cosmic muons, when one of the parts of a track is reconstructed erroneously or there are random coincidences with events involving two uncorrelated leptons. The analysis showed that, in most cases, such pairs of muons are directed oppositely to each other, and hence the additional criterion

$$\Delta R_{\cos} = \sqrt{\left(|\phi| - \pi\right)^2 + (\eta_1 + \eta_2)^2} < 0.01$$

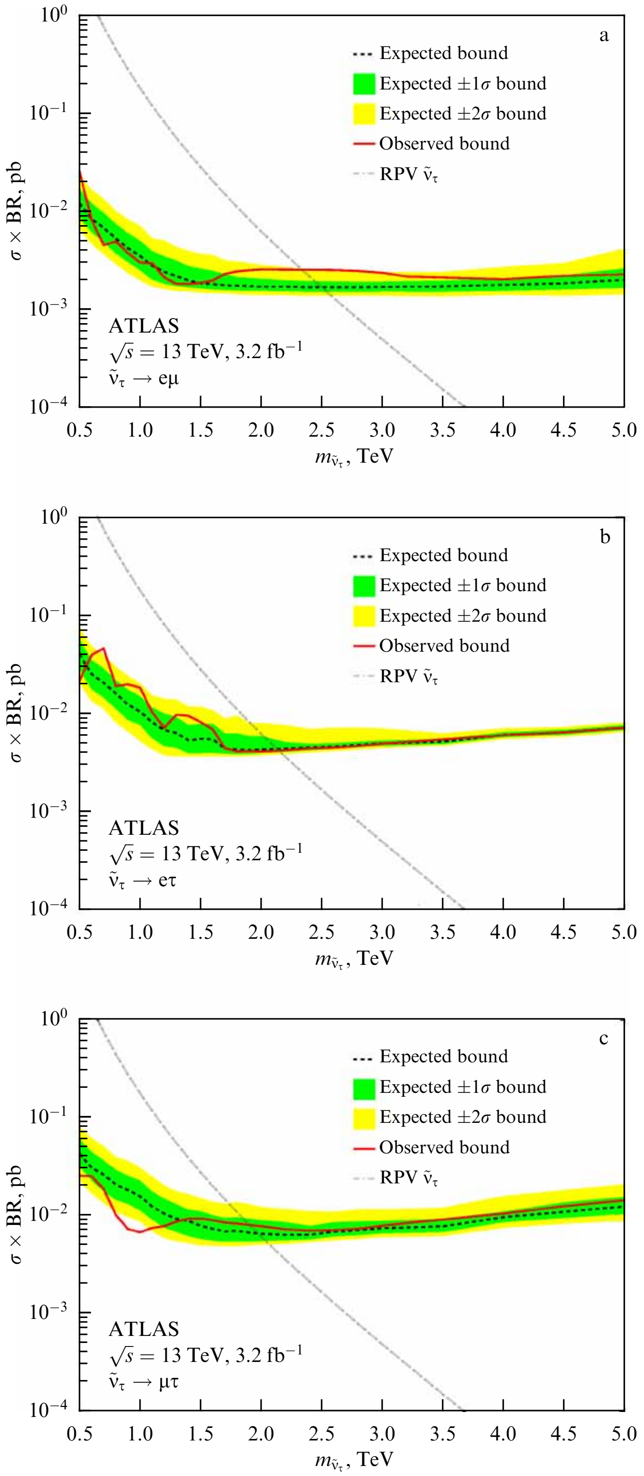

Figure 10. (Color online.) Observable upper bounds for the tau-slepton production cross section in the pair decay channel (a) $e^{\pm}\mu^{\mp}$, (b) $e^{\pm}\tau^{\mp}$, and (c) $\mu^{\pm}\tau^{\mp}$, with $\sigma(pp \to \tilde{\nu}_\tau) \times BR(\tilde{\nu}_\tau \to e\mu/e\tau/\mu\tau)$ at a 95% confidence level as functions of tau-slepton mass $m_{\tilde{\nu}_\tau}$ at $\sqrt{s} = 13$ TeV. The expected bounds are shown with the total error taken into account within ± 1 and ± 2 standard deviations. Theoretical cross sections of the process [70, 71] with total errors [78] are also given.

allows effectively separating these events in the signal region (SR). In addition, this variable was used to determine the background normalization in the range $0.0015 < \Delta R_{\cos} < 0.004$ and to extrapolate the normalization coefficient to the range $\Delta R_{\cos} > 0.01$. As a result, for a squark mass of 700 GeV and a neutralino mass of 50–500 GeV, the lifetimes corresponding to $c\tau = 1-600$ mm were excluded. Similarly, for a squark mass of 1.6 TeV and a neutralino mass of 1.3 TeV, the values $c\tau = 3-100$ mm were excluded [79].

The best lower bounds for the tau-sneutrino mass in a similar decay channel into an $e^{\pm}\mu^{\mp}$ pair, established in the CMS experiment, were obtained by analyzing data collected at $\sqrt{s} = 8$ TeV, corresponding to the integrated luminosity 19.7 fb^{-1} [80]. Under different assumptions about the values of the coupling constants, $\lambda_{132} = \lambda_{231} = \lambda'_{311} = 0.01$, and $\lambda_{132} = \lambda_{231} = 0.07$, and $\lambda'_{311} = 0.11$, the respective lower bounds for the tau-sneutrino mass were 1280 and 2300 GeV.

To conclude this section, we note that other experimental data can also be used to impose bounds on the RPV constants λ that determine the probabilities of decay channels into a pair of different leptons at LHC energies. For example, the upper bounds of the coupling constants λ_{132} and λ_{233} can be calculated from the constraints on the $e-\mu-\tau$ universality of the coupling constants of quarks and leptons to the W-boson and ratios of the tau-lepton decay widths $\Gamma(\tau \to e\nu\bar{\nu})/\Gamma(\tau \to \mu\nu\bar{\nu})$ [81, 82] or from a constraint on the electron-neutrino mass, for example, on the λ_{133} coupling constant [30, 83–91]:

$$|\lambda_{131/132/23k}| < 0.03\left(\frac{m_{\tilde{e}_{Rk}}}{M_W}\right),$$

$$|\lambda_{133}| < 7.5 \times 10^{-4}\left(\frac{M_{SUSY}}{M_W}\right)^{1/2},$$

where M_{SUSY} is the SUSY breaking scale. For example, for the tau-sneutrino mass of 1.3 TeV (2.3 TeV), we obtain $\lambda_{131/132/23k} < 0.49$ (< 0.86) and $\lambda_{133} < 3.0 \times 10^{-3}$ $(< 4.0 \times 10^{-3})$.

4. Multilepton final states

Registration of pp-interaction events with a large multiplicity of leptons (in this case, at least four) (Fig. 11) typically implies not only a long chain of successive decays of a sufficiently heavy initially produced particle but also the requirement that the final-state energy of all the decay products exceed some trigger threshold of detector registration.

The first search for a multilepton signature of this kind was performed at $\sqrt{s} = 7$ TeV with the ATLAS data corresponding to the integrated luminosity of 4.7 fb^{-1} [93]. This was one of the first studies using the concept of a 'simplified SUSY model.' The so-called model-independent approach was used in which only the required SUSY particle with a fixed decay chain was generated; in other words, from the entire spectrum of SUSY particles, only masses of 2 to 4 particles were specified, which allowed significantly simplifying the derivation of bounds for various mass spectra of SUSY particles [94]. Another more common scenario, considered in [93], was the MSUGRA/CMSSM (Minimal SUperGRAvity Standard Model/Constrained Minimal Supersymmetric Standard Model) with a limited set of parameters: $m_0 = A_0 = 0$ and $\mu > 0$ [95].

Only electrons and muons, including leptonic decays of tauons, were considered to be leptons. Two sets of event selection criteria were used, both of which had to contain at least four leptons with $p_T > 10$ GeV, but the additional criterion $E_T^{miss} > 50$ GeV was used for one of these selections (for high sensitivity in the range of low masses of the produced

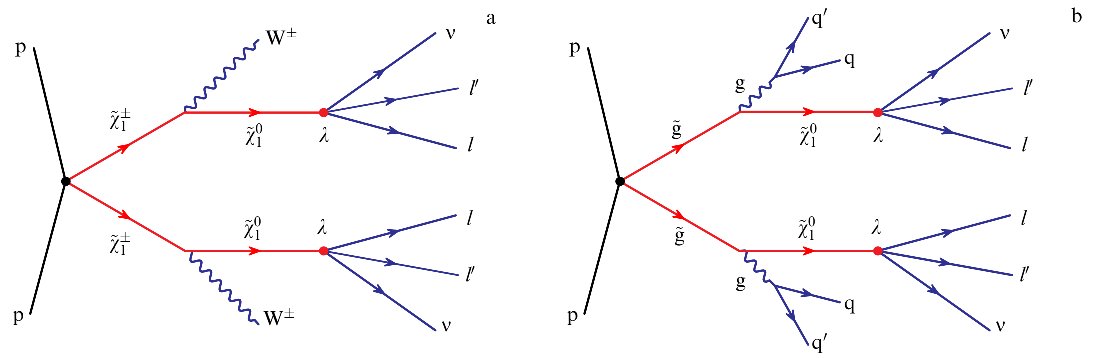

Figure 11. (Color online.) Production of a pair of (a) gauginos and (b) gluinos and their RPC transformation into neutralinos followed by RPV decay of the neutralino into three leptons (see Fig. 2), $\tilde{\chi}_1^0 \to ll\nu$, with 100% probability. (From [92].)

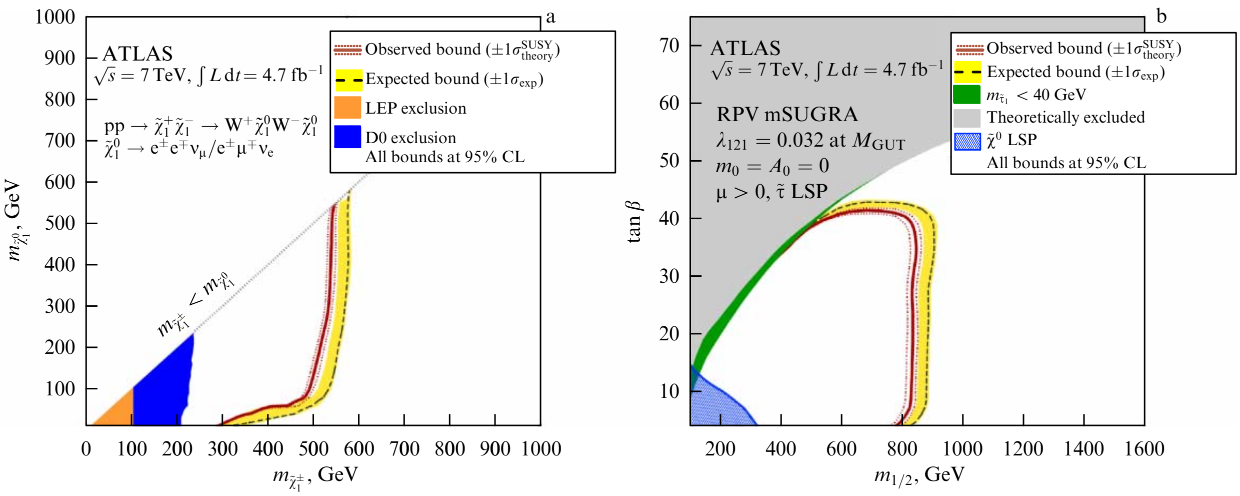

Figure 12. (Color online.) Observed and expected bounding contours for (a) the 'simplified model' and (b) MSUGRA/CMSSM at a 95% confidence level. Expected and observed bounds were calculated without taking the error in the SUSY particle production cross section into account. Yellow strip shows range of $\pm 1\sigma$ for the experimental error in the expected bound (black dashed curve). Red dotted curve shows range of $\pm 1\sigma$ of the theoretical signal error for the observed bound (red solid curve). Linear interpolation was used to take signal grid discreteness into account. From two sets of the event selection criteria, the one giving the smaller bound [93] was used. Bounds obtained previously in LEP experiments [96] and in the D0 experiment [97] are also shown. Bound for stau production with $m < 40$ GeV was obtained from the Z-boson decay width in LEP experiments [98].

particle), and the effective mass

$$m_{\mathrm{eff}} = \sum_i^{\mathrm{jet}} p_{\mathrm{T}}^i + \sum_i^{\mathrm{lep}} p_{\mathrm{T}}^i + \sum_i^{\mathrm{phot}} p_{\mathrm{T}}^i$$

(the scalar sum of the transverse momenta of all reconstructed objects in the event) was required to exceed 300 GeV in the other (for high sensitivity in the range of large masses of the produced particle).

Each oppositely charged lepton pair with the same lepton number was varied with respect to the invariant Z-boson mass in the range of ± 10 GeV. Background processes yielding a similar signature in the final state, ZZ, $\mathrm{t\bar{t}Z}$, and $\mathrm{t\bar{t}WW}$, were simulated by the Monte Carlo method. The processes WZ, $\mathrm{t\bar{t}}$, $\mathrm{t\bar{t}W}$, and WW and the associative single t-quark or Z-boson production with hadronic jets or photons, in which the final-state signature can repeat only as a result of erroneous reconstruction of a lepton from the leptonic decay of a b or c quark or from photon conversion, were determined by 're-weighing' using data. As can be seen from Fig. 12, which shows the observed and expected bounding contours for the 'simplified model' (Fig. 12a) and MSUGRA/CMSSM (Fig. 12b) at a 95% confidence level, it was possible to significantly improve the results obtained previously in experiments at the LEP (Large Electron–Positron) collider [96, 98] and in the D0 experiment [97].

Similarly to the analysis with a $\mathrm{e}^{\pm}\mu^{\mp}$-pair final state (see Section 3), this analysis was later extended to include hadronic decay channels of the tau lepton. Accordingly, the number of signal search regions increased to three at $\sqrt{s} = 8$ TeV and the integrated luminosity of 20.3 fb^{-1} [92] and to four at $\sqrt{s} = 13$ TeV and the integrated luminosity of 36.1 fb^{-1} [99], depending on the multiplicity of hadron-decayed tauons ($N_{\tau_{\mathrm{had}}} \geqslant 0$, $\geqslant 1$, or $\geqslant 2$) in the event. In addition, in the data analysis at $\sqrt{s} = 8$ TeV in all signal search regions, only the constraint $E_{\mathrm{T}}^{\mathrm{miss}} > 50$ GeV worked well as an additional criterion, whereas, at $\sqrt{s} = 13$ TeV, the best sensitivity was achieved using the m_{eff} criterion at 600, 700, and 650 GeV for the respective events with $N_{\tau_{\mathrm{had}}} = 0$, $\geqslant 1$, and $\geqslant 2$. The fourth signal search region at $\sqrt{s} = 13$ TeV was the range with $N_{\tau_{\mathrm{had}}} = 0$ and the high criterion $m_{\mathrm{eff}} > 1100$ GeV. As can be seen from Fig. 13, all the measures taken allowed increasing the bounds for the data at $\sqrt{s} = 13$ TeV by a factor of 1.5 to 2 compared with the bounds for data at $\sqrt{s} = 8$ TeV.

The best bounds for gluino and squark masses in the CMS experiment in a channel with three or four final-state leptons (e, μ, and τ) are established in an analysis of data obtained at

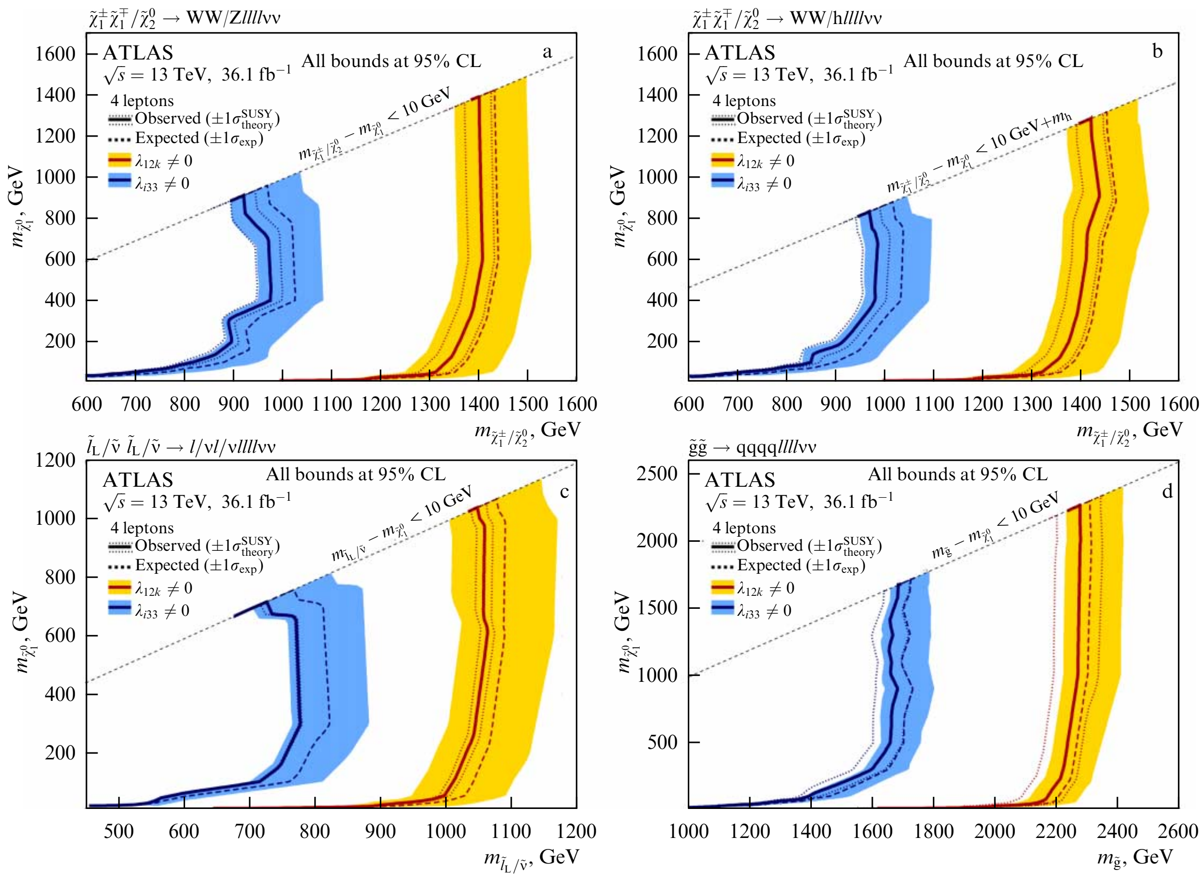

Figure 13. (Color online.) Observed and expected bounding contours for 'simplified models' at a 95% confidence level. Models with $\lambda_{12k} \neq 0$ include decays only into electrons and muons, and models with $\lambda_{i33} \neq 0$, only into a tauon and a muon or an electron. From two sets of event selection criteria, the one giving the smaller bound was used [99].

$\sqrt{s} = 7$ TeV and the integrated luminosity of 4.98 fb^{-1} and at $\sqrt{s} = 8$ TeV and the integrated luminosity of 19.5 fb^{-1} [100, 101]. For models with only lepton RPV, $\lambda_{e\mu\tau} > 0.05$, gluino masses were excluded in the range from 600 GeV to 1 TeV for the squark mass from 900 GeV to 2 TeV, and in the range from 600 GeV to 2 TeV for squark masses from 900 GeV to 1200 GeV. Squark masses for the gluino mass range from 1 TeV to 1.6 TeV were bounded from 600 GeV to 1200 GeV, and for the gluino mass from 600 GeV to 1 TeV, squark masses from 600 GeV to 2 TeV were excluded for models with only hadronic RPV, $\lambda''_{\rm uds} > 0.05$.

In Section 3, we mentioned the possibility of imposing constraints on various violating constants λ for the corresponding decays using other experimental data, including λ_{23k} and λ_{133}. In addition, the bounds for a violating constant, e.g., λ_{12k}, can also be calculated from the constraints on the universality of processes occurring via charged currents and the constants of quark and lepton couplings to the W boson [81, 82]:

$$\lambda_{12k} < 0.01\,\frac{m_{\tilde{d}_{{\rm R}k}}}{M_{\rm W}}\,.$$

The upper bound for the violating constants, e.g., λ_{12k}, for a squark mass of 1 TeV (2 TeV) is then $\lambda_{12k} < 0.12$ (< 0.25).

5. Multijet decays of gluino or squark pairs

In SUSY models, proton–proton production of gluino pairs pp $\to \tilde{g} + \tilde{g}$ or squarks pp $\to \tilde{q} + \tilde{q}$, due to their large mass, typically occurs with a high multiplicity of secondary high-energy quarks.

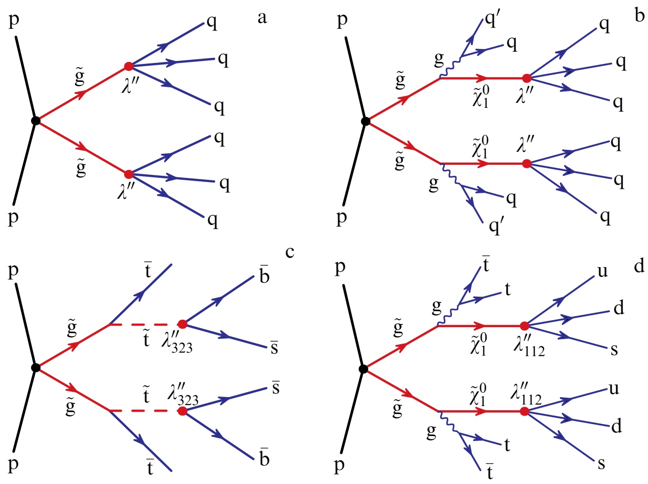

Figure 14. (Color online.) Decays, proportional to the λ'' constant, of a gluino pair into hadron jets, both direct and via neutralinos and $\tilde{t}$ squarks.

The first search for this type of RPV processes was carried out by the ATLAS collaboration only under the assumption of (sequential) gluino decay into three quarks $\tilde{g} \to \tilde{q}q \to qqq$, where the second decay is proportional to λ'', an RPV parameter in the hadron sector. Two such gluino decays would produce a signal event with six hadron jets in the final state (Fig. 14a).

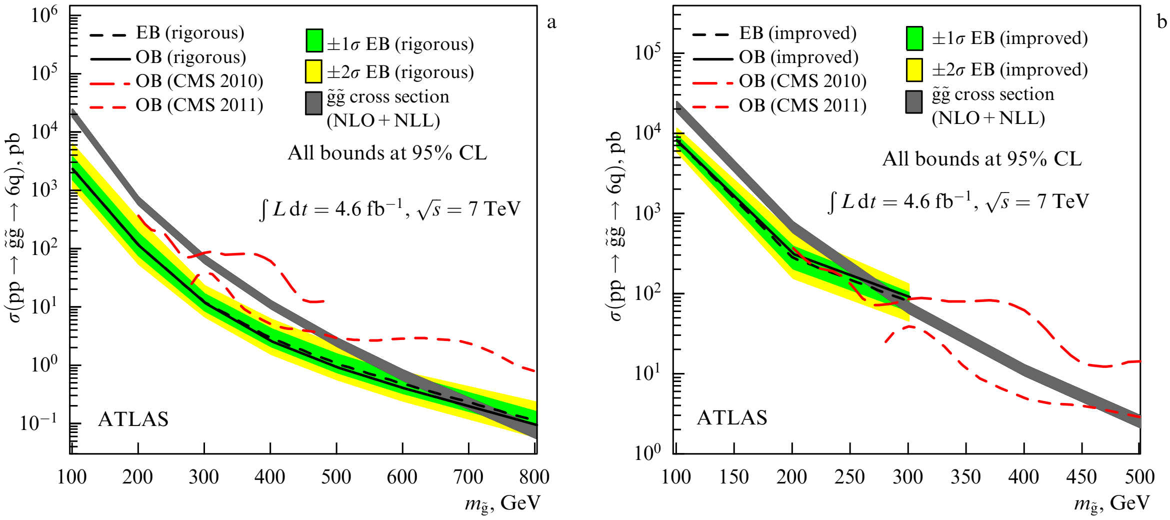

Figure 15. (Color online.) Observed bounds (OB) and expected bounds (EB) (95% confidence level) of cross sections of the production of (a) six jets and (b) two large jets. For comparison, CMS results are shown for 2010 and 2011 data corresponding to integrated luminosity 35 pb^{-1} and 5 fb^{-1} [105].

These parameters correspond to the violating constants λ''_{ijk}, the upper bounds for which can be deduced from various bounds for the results of other experiments. For example, the λ''_{3jk} upper bound can also be established from corrections for Z-boson decay into a pair of light fermions [102, 103],

$$\lambda''_{3jk} < 0.65\,\frac{m_{\tilde{q}_{Rk}}}{M_W}\,,$$

and the λ''_{112} upper bound can be deduced from nonobservation of double nucleon decay [104]. Because the lower bound for the lifetime of such a decay is $\tau_{NN} > 10^{30} - 10^{33}$ s [38], we have

$$\lambda''_{121} < 10^{-15}\left[\frac{\tilde{\Lambda}}{(m_{\tilde{g}} m_{\tilde{q}}^4)^{1/5}}\right]^{-5/2},$$

where $\tilde{\Lambda}$ is the effective parameter of the nuclear structure.

Depending on the energy of the produced gluino, either the quarks can form six hadron jets or the emission (momentum) direction of the quarks is strongly collimated with the direction of the gluino (when the gluino transverse momentum is sufficiently large, $p_T^{\tilde{g}} \gtrsim 2m_{\tilde{g}}$), in which case two large-radius high-energy jets form (Fig. 14a). This largely applies to search regions for gluinos of a lower mass (up to 500 GeV).

The first analysis using this signature was already carried out at $\sqrt{s} = 7$ TeV and data corresponding to an integrated luminosity of 4.7 fb^{-1} [105]. In the case of six hadronic jets, the main background is given by quantum chromodynamics (QCD) processes of multiple production of quarks and gluons. This background was predicted by re-weighing the number of hadronic jets in events from the low-multiplicity region to the SR with six jets with a transverse momentum ranging from 80 to 160 GeV, depending on the gluino mass.

The selection of events with two large-radius jets was divided into two search regions. In the first, for relatively small gluino masses, each jet is required to have $p_T^{\rm jet} > 200$ GeV and the invariant mass $m_{J_1,J_2}^{\rm jet} > 60$ GeV. The second search region was optimized for large gluino masses with the transverse momentum of each jet above 350 GeV and the invariant mass above 200 GeV.

To suppress the multijet background QCD processes, each large jet was checked for the number of 'subjets' inside it (the so-called τ_{32} criterion in [105]). It was the inversion of this criterion, together with the criterion imposed on the invariant mass, that allowed applying the ABCD background estimation method, whose essence is to preserve the ratios of background events in regions with inverted criteria for τ_{32} and $m_{J_1,J_2}^{\rm jet}$ and background events in the signal-event search region. As can be seen from Fig. 15, the best bound for the cross section for the production of a gluino pair decaying into six quarks was established as a result of the analysis of events with six jets in the final state in the gluino mass range of 100–500 GeV.

With the transition to data collected at $\sqrt{s} = 8$ TeV and the integrated luminosity of 20.3 fb^{-1}, it became possible to expand the analysis by adding the reconstruction of a hadron jet initiated by a b quark (b-jet) and vetting signal leptons [106]. A curious feature of this analysis is that the SRs were not orthogonal to each other. Nineteen SRs of two types were considered: a multijet with b-jets and a multijet with large jets. In the SRs of the first type, there were six regions with $N_j = 8$ and 9 jets with $p_T^{\rm min} = 50$ GeV, and the number of b-jets was 0, 1, or $\geqslant 2$ with $p_T > 40$ GeV, and, similarly, six more regions with $N_j = 7$ and $\geqslant 8$ jets with $p_T^{\rm min} = 80$ GeV. The 13th region of this type was the one without any criteria regarding the presence of b-jets, $N_j \geqslant 10$ and $p_T^{\rm min} = 50$ GeV. The same event could then be present in regions with different $p_T^{\rm min}$ and the b-jets did not have to be from among the signal jets. Similarly, events were selected for second-type regions with $N_j \geqslant 8$, $\geqslant 9$, and $\geqslant 10$ jets and with $p_T^{\rm min} = 50$ GeV, but the remaining jets in the event with $p_T > 20$ GeV were checked for the possibility of combining them into large jets. Then, for each value of N_j, a criterion was applied involving the scalar sum of the invariant masses of all large ($R = 1.0$) jets in the event:

$$M_J^{\Sigma} \equiv \sum_j m_j^{R=1.0} > 340 \text{ GeV} \quad \text{and} \quad M_J^{\Sigma} > 420 \text{ GeV}\,.$$

As can be seen from the selection criteria, SRs of this type were not orthogonal either to each other or to the regions of the first type. For all regions, the criterion for resolution of

$\delta E_{\mathrm{T}}^{\mathrm{miss}}$ was used,

$$\delta E_{\mathrm{T}}^{\mathrm{miss}} = \frac{E_{\mathrm{T}}^{\mathrm{miss}}}{\sqrt{H_{\mathrm{T}}}} > 4\ \mathrm{GeV}^{1/2}\,,$$

where

$$H_{\mathrm{T}} = \sum_j p_{\mathrm{T}}^j \tag{11}$$

is the scalar sum of transverse momenta of all jets in the event. In this case, H_{T} is obtained by summing only over jets with $p_{\mathrm{T}} > 40$ GeV. Background events from processes of direct $\mathrm{t\bar{t}}$-pair production and $\mathrm{W,Z}$ + jets with hadronic decays and multijet QCD processes were estimated by extrapolating the normalization coefficient for events in the data, except all other events, from the region with $N_j = 6$ (7 for regions with large jets) and the inverted criterion $\delta E_{\mathrm{T}}^{\mathrm{miss}} < 1.5\ \mathrm{GeV}^{1/2}$ for distributions with respect to $\delta E_{\mathrm{T}}^{\mathrm{miss}}$.

In addition, all signal events also contain events with leptonic decays of $\mathrm{t\bar{t}}$ pairs, $\mathrm{W} \to l\nu$ + jets and $\mathrm{Z} \to \nu\nu$ + jets, or a single t-quark production due to a soft or unreconstructed lepton. Such background events from processes of a $\mathrm{t\bar{t}}$ pair, $\mathrm{W} \to l\nu$, were evaluated using selection criteria similar to those for each SR, but the lepton was considered a jet. If the lepton p_{T} satisfies the $p_{\mathrm{T}}^{\mathrm{min}}$ condition, then the multiplicity of jets in the event increased and the lepton was taken into account in both $E_{\mathrm{T}}^{\mathrm{miss}}$ and H_{T}. Background events from $\mathrm{Z} \to \nu\nu$ + jets were estimated from simulations.

The final fitting of background events to the data was carried out simultaneously in all regions of a given type with a given $p_{\mathrm{T}}^{\mathrm{min}}$. The results were interpreted in a 'simplified model' of direct production of a gluino pair decaying via a stop quark $\tilde{\mathrm{g}} \to \tilde{\mathrm{t}}(\to \mathrm{bs})\mathrm{t}$ (Fig. 14d). Figure 16 shows that gluino masses below 900 GeV are ruled out at a 95% confidence level when the stop-quark mass is in the range of 400–1000 GeV.

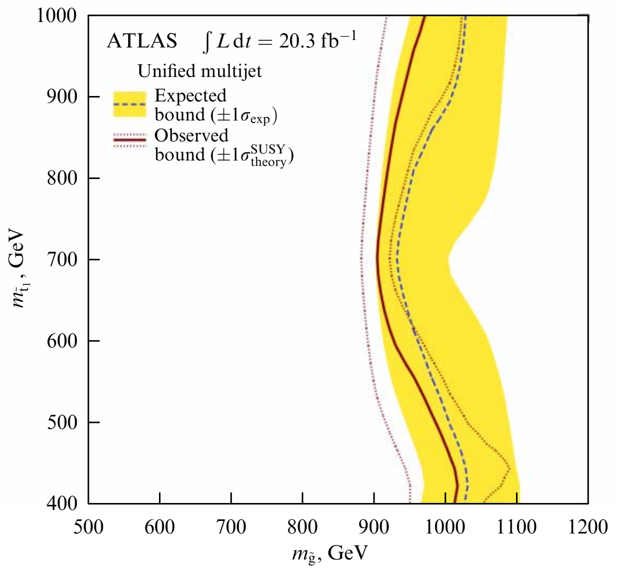

Figure 16. (Color online.) Observed and expected bounds (95% confidence level) for the 'simplified model' of gluino pair production with RPV decay $\tilde{\mathrm{g}} \to \mathrm{t}\tilde{\mathrm{t}}(\to \mathrm{bs})$. For the $\pm 1\sigma$ error of the expected bound, shown in yellow, the theoretical error of the production cross section was not taken into account. The dotted lines show changes in the observed bound with an increase or decrease in the theoretical signal production cross section within the theoretical error. (From [106].)

This analysis was later repeated with a larger number of SRs [107]: 48 SRs were used with simultaneous variation in (a) the jet multiplicity ($N_j \geqslant 6$ or 7); (b) values of the minimum transverse momentum of the jet in the range of 80–220 GeV with a 20-GeV step; (c) the minimum number of b-jets in the event equal to 0, 1, and 2. Because the SRs with large and small jets were then again considered separately, the method for estimating the background did not change from that in the previous analysis at $\sqrt{s} = 7$ TeV [105].

In addition, the process of estimating background events in the SR was automated by extrapolating normalization coefficients from the control region (a kinematic region with no signal) with a simultaneous evaluation of the systematic errors and their correlations, which allowed significantly increasing the number of kinematic search regions of New Physics.

This was done for a part of the analysis assuming the presence of four large-radius hadronic jets with $p_{\mathrm{T}}^4 > 100$ GeV, with an additional criterion imposed on the scalar sum of the invariant masses of the four jets, M_J^{Σ}. In the control region with exactly three large jets with $p_{\mathrm{T}} > 100$ GeV and $|\eta| > 2.5$, mass distributions for each jet were constructed depending on its p_{T} and η, such that 2500 distributions were obtained and the normalization coefficients were determined accordingly. The obtained coefficients were verified in kinematically orthogonal control and 'validation' regions using the inverted criterion for the difference between the pseudorapidities of two jets leading in the transverse momentum: $|\eta| > 1.4$ and $1 < |\eta| < 1.4$.

For three SRs, this criterion implied that these jets are closer to each other ($|\eta| > 0.7$). The first of the three SRs was the most universal for $p_{\mathrm{T}}^3 > 250$ GeV and $M_J^{\Sigma} > 650$ GeV. The other two served to increase the sensitivity of the analysis in the region of low and high gluino masses with the respective criteria $p_{\mathrm{T}}^3 > 100$ and 200 GeV and the same $M_J^{\Sigma} > 350$ GeV. As can be seen from Fig. 17a, an increase in the number of statistics allowed establishing the bounds for the cross section of gluino pair production with six jets in the final state for gluino masses up to 1300 GeV, and for the model with 10 jets in the final state, variants with the gluino mass below 900 GeV and the neutralino mass $m_{\tilde{\chi}_1^0} < 600$ GeV were excluded (Fig. 17b).

Subsequently, at $\sqrt{s} = 13$ TeV and the integrated luminosity of 36.1 fb^{-1}, only part of the analysis was repeated with large jets and M_J^{Σ} taken as the principal variable for separating the signal from the background, but a significant addition came from SRs with the selection of at least one b-jet and more than four or five large jets [108]. In addition, the statistical error of the jet mass distributions from the control region was regarded as a systematic error in the SR, and the normalization itself was carried out in the range $200 < M_J^{\Sigma} < 600$ GeV.

As can be seen from Fig. 18a, the cross section bound for direct production of a gluino pair decaying into six quarks could be improved by a factor of almost three at low gluino masses and a bound could be imposed on the gluino mass up to 1800 GeV. For the SUSY model with 10 jets in the final state, the gluino mass bounds were also almost doubled, and gluino masses less than 1875 GeV and neutralino masses greater than 200–400 GeV were excluded.

At the same time, further analysis at $\sqrt{s} = 13$ TeV and the integrated luminosity of 36.1 fb^{-1} with a large number of hadronic jets and b-jets was extended by the occurrence of t quarks, $\tilde{\mathrm{t}}$ squarks, and a lepton (e or μ) in the decay chain of a

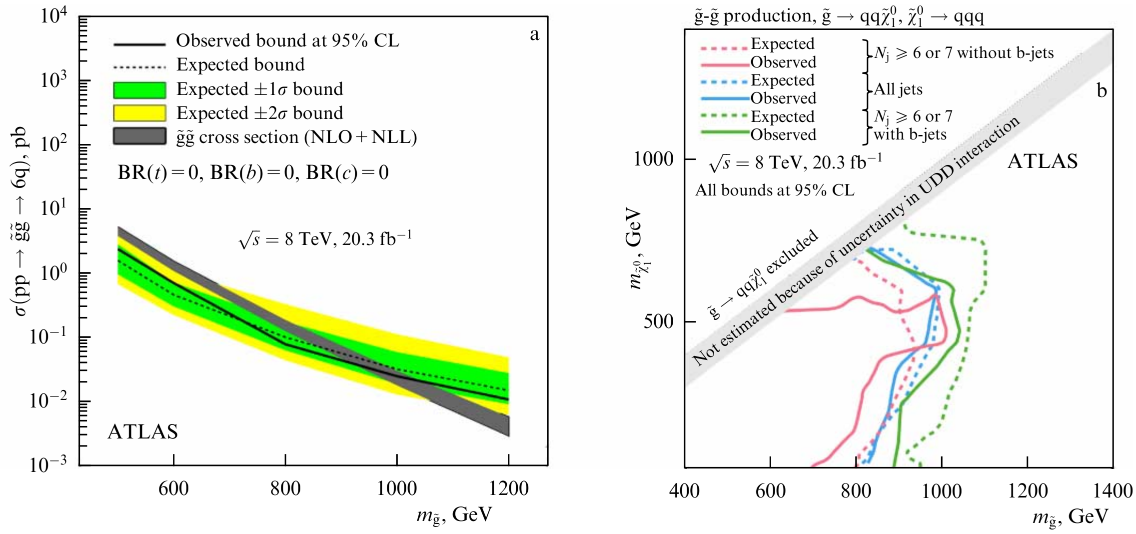

Figure 17. (Color online.) Observed and expected bounds (confidence level 95%) of the cross sections for (a) production of six jets through two gluinos and (b) for all considered variants of the analysis of the SUSY model with 10 jets in the final state [107].

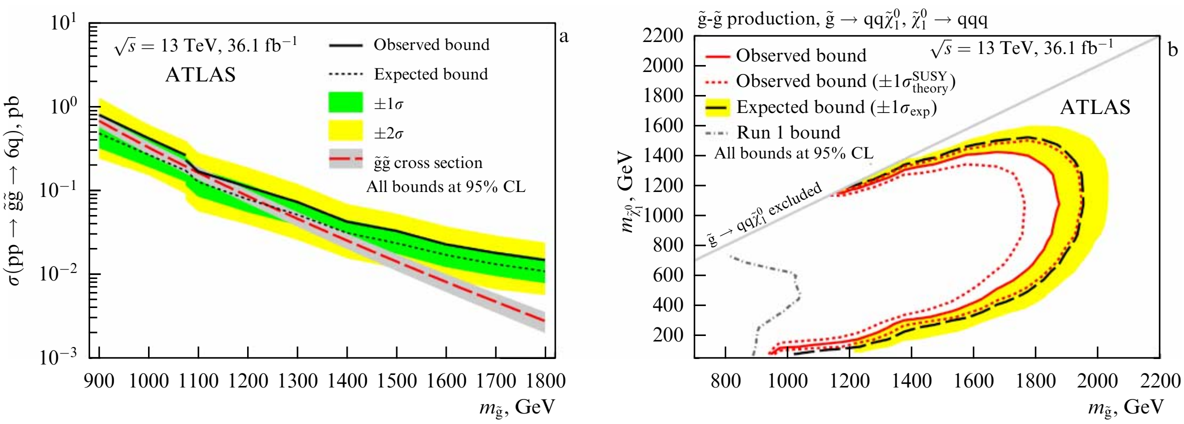

Figure 18. (Color online.) (a) Expected and observed bounds for the cross section of direct gluino pair production with six jets in the final state at a 95% confidence level. (b) Expected and observed bounds for the cross section of direct gluino pair production in a SUSY model with 10 jets in the final state at a 95% confidence level [108]. Also shown is the observed bound obtained in the previous analysis at $\sqrt{s} = 8$ TeV and the integrated luminosity 20.3 fb^{-1} [107].

gluino pair and hence by the additional requirement that an isolated lepton with $p_{\mathrm{T}} > 30$ GeV be present in the event [109].

All control and SRs in this case were first divided into three categories according to the lower p_{T} threshold of the jet given by 40, 60, and 80 GeV. Depending on the lower threshold, from 5 to 10–12 jets were present in the event. To estimate the background, distributions over the number of b-jets from zero to at least four were used.

The main backgrounds were the W/Z + jets production processes, production of a $\mathrm{t\bar{t}}$-quark pair, and multijet processes. To estimate the background of the last type, a matrix method was used based on relaxing the lepton identification criterion and the ratio of the number of primary to secondary leptons that passed the corresponding identification criteria. To estimate the contribution to the SRs from the first two background processes, the method of extrapolation of normalization coefficients from the region with a low multiplicity of jets was used.

For the W/Z + jets process, this was done by taking the shape of the b-jet multiplicity distribution from Monte Carlo simulation results, and for the $\mathrm{t\bar{t}}$-process, by subtracting all other background processes from the data. A total of 18 SRs were used: six for each threshold with respect to p_{T} of the jet (40, 60, and 80 GeV) with the respective jet multiplicity intervals of 10–12, 8–10, and 8–10 for each threshold value, and the b-jet multiplicities 0 and $\geqslant 3$. Events with two b-jets were not considered, because a high proportion of background events from the $\mathrm{t\bar{t}}$-process significantly reduces the sensitivity to signal processes.

Thus, under the assumption of direct RPC production of a gluino pair ($\mathrm{pp} \to \tilde{\mathrm{g}}\tilde{\mathrm{g}}$) followed by RPV decays $\tilde{\mathrm{g}} \to \mathrm{t\bar{t}}\tilde{\chi}_1^0 \to \mathrm{t\bar{t}uds}$, $\tilde{\mathrm{g}} \to \bar{\mathrm{t}}\tilde{\mathrm{t}} \to \bar{\mathrm{t}}\mathrm{b\bar{s}}$ (Fig. 14c, d), and $\tilde{\mathrm{g}} \to \mathrm{q\bar{q}}\tilde{\chi}_1^0 \to \mathrm{q\bar{q}q\bar{q}}l\nu$, the gluino mass bounds were respectively set at 2.1, 1.65, and 1.8 TeV at a 95% confidence level (Fig. 19).

The CMS collaboration excluded gluino masses up to 1100 GeV in the channel of a pair of produced gluinos decaying into 10 final-state quarks by analyzing data obtained at $\sqrt{s} = 8$ TeV and the integrated luminosity of 19.6 fb^{-1} [111]. Both light and heavy quarks were considered.

Because the lower bound was set only for the gluino mass, we set the squark mass $m_{\tilde{\mathrm{d}}_{\mathrm{R}k}} = 1$ TeV to calculate the upper bound for the R-violating constants. For the 1 TeV gluino mass, this then yields the constraints $\lambda''_{3jk} < 8.1$ and $\lambda''_{121} < 56$.

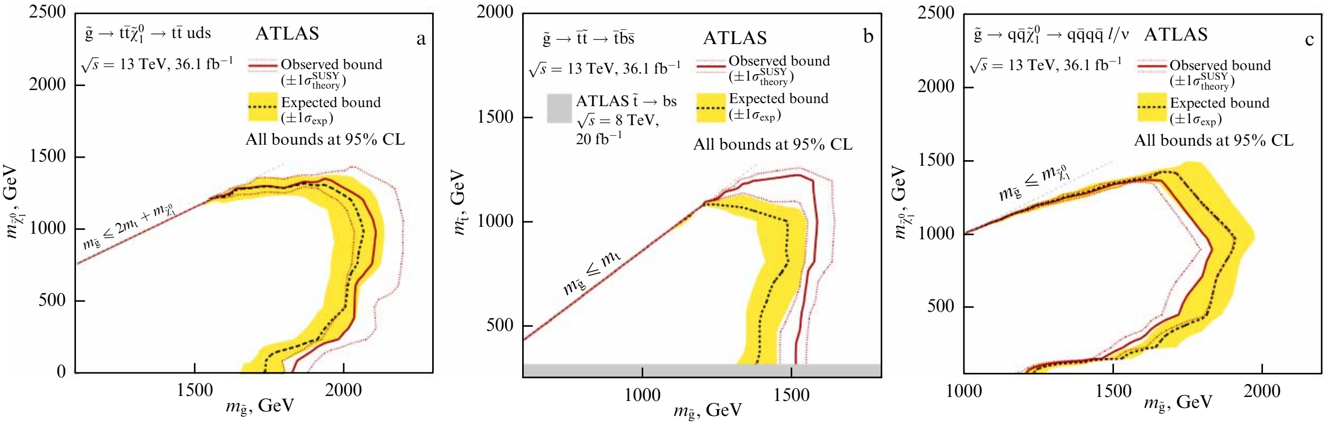

Figure 19. (Color online.) Observed and expected contours of $\tilde{g}$ and χ_1^0 excluded masses in the framework of an RPV scenario, obtained using 'simplified' gluino pair production models with dedicated channel decay. For the error $\pm 1\sigma$ of the expected bound shown with a strip, the theoretical error of the signal production cross section was not taken into account. Dotted curves show changes in the observed bound with an increase or decrease in the theoretical cross section for signal production within the theoretical error. All bounds are obtained at a 95% confidence level. Diagonal lines show kinematic bound for a given decay channel. Bound for the $\tilde{g} \to \bar{t}\,\tilde{t} \to \bar{t}\bar{b}\bar{s}$ channel, obtained at $\sqrt{s} = 8$ TeV and the integrated luminosity 20 fb^{-1} [110], is shown in gray [109].

6. Multijet events with two identically charged leptons or three leptons

The first analysis of events with a large number of hadron jets accompanied by two or three leptons, with the aim to interpret them within the RPV–SUSY scenario, was carried out by the ATLAS collaboration at $\sqrt{s} = 8$ TeV and the integrated luminosity of 20.3 fb^{-1} [112].

The signal event selection criterion was the requirement that there be at least three leptons or two equally charged leptons (Fig. 14d), at least five hadron jets with $p_{\rm T} > 40$ GeV, and at least three b-jets, with the effective sum of the $p_{\rm T}$ for all leptons, all jets, and $E_{\rm T}^{\rm miss}$ being $m_{\rm eff} > 350$ GeV [112].

With this selection, the main backgrounds were taken as events with an erroneously reconstructed electron charge, secondary leptons from decays of SM particles, or, for example, from jets erroneously reconstructed as a lepton.

The probability of an erroneous reconstruction of the electron charge was estimated from $Z/\gamma^* \to$ ee events, when the invariant Z-boson mass was reconstructed in the ± 10 GeV window for a pair of oppositely and equally charged electrons. The probability of an erroneous reconstruction of the electron charge was a free parameter of fitting the two obtained distributions to the data for different values of $p_{\rm T}$ and the electron pseudorapidity η. The background from the erroneously reconstructed lepton was estimated using the matrix method described above. The effect of all other background processes was determined by simulations. The events selected in this way were interpreted within only two SUSY scenarios. In the first one, direct RPC production of a gluino pair was assumed with its RPV decay via the $\tilde{g} \to \tilde{t}_1(\to {\rm bs})$t channel due to $\lambda''_{332} \neq 0$, and, in the second scenario, the SUSY model with bilinear RPV [113] was used for $\mu_j \neq 0$ in (4).

We can see from Fig. 20 that gluino masses less than 900 GeV and stop quark masses in the range of 300–1000 GeV are excluded in the first model, and the parameter values $m_{1/2} > 500$ GeV with $m_0 < 2.1$ TeV are excluded in the second model at a 95% confidence level.

At $\sqrt{s} = 13$ TeV and the integrated luminosity of 36.1 fb^{-1}, the analysis was extended further by the requirement that the event contain at least 3 to 6 jets with $p_{\rm T} > 50-40$ GeV and from 0 to 2 b-jets, as well as $m_{\rm eff} > 1200-2200$ GeV [114]. The methods for estimating background events remained mostly the same, except that the template method was additionally applied to the matrix method for estimating the background from erroneously reconstructed leptons, with the template method based on simulating the kinematic distributions of erroneously reconstructed leptons in the production of $t\bar{t}$ pairs and W/Z + jets.

In the kinematic region with $E_{\rm T}^{\rm miss} > 40$ GeV, containing at least two ($\geqslant 2$) equally charged leptons and at least two ($\geqslant 2$) jets, distributions were constructed for five possible options for the production of electrons and muons: from b-jets, from other jets, and, for conversion electrons, from photons.

Subsequently, these distributions were also subdivided according to the presence or absence of a b-jet in the event. The fraction of each option for the origin of such a lepton was a free parameter in fitting the data. Because the matrix method and the template method were in good agreement with each other, they were combined. The results were interpreted in four variants of RPV decays of a gluino pair (Fig. 21a, b),

$$\tilde{g} \to \tilde{t}(\to \bar{b}\bar{d})\bar{t}\,, \quad \tilde{g} \to \tilde{t}(\to \bar{s}\bar{d})\bar{t}\,, \quad \tilde{g} \to qq\tilde{\chi}_1^0(\to lqq)\,,$$
$$\tilde{g} \to qq\tilde{\chi}_1^0(\to {\rm uds})\,,$$

and in two variants of RPV decays of a pair of $\tilde{d}_{\rm R}$ squarks after their RPC production (via a t-channel gluino exchange) (Fig. 21c),

$$\tilde{d}_{\rm R} \to \bar{b}\bar{t}\,, \quad \tilde{d}_{\rm R} \to \bar{s}\bar{t}\,.$$

Figure 22 shows that, in RPV–SUSY scenarios of this kind, the $\tilde{d}_{\rm R}$-squark mass up to 500 GeV is excluded, and gluino masses up to 1.3 TeV are excluded.

Considered at $\sqrt{s} = 13$ TeV and the integrated luminosity of 139 fb^{-1} in this channel was the presence of at least two identically charged leptons (as previously) and six jets with $p_{\rm T} > 40$ GeV, but already inclusive with respect to the number of b-jets [115]. To additionally suppress the background events originating mainly from the WZ + jets, tV-, $t\bar{t}$VV-, and 3 to 4 t-quark processes, $m_{\rm eff}$ was required to be greater than 2400 eV. Here, V denotes a vector W or Z boson.

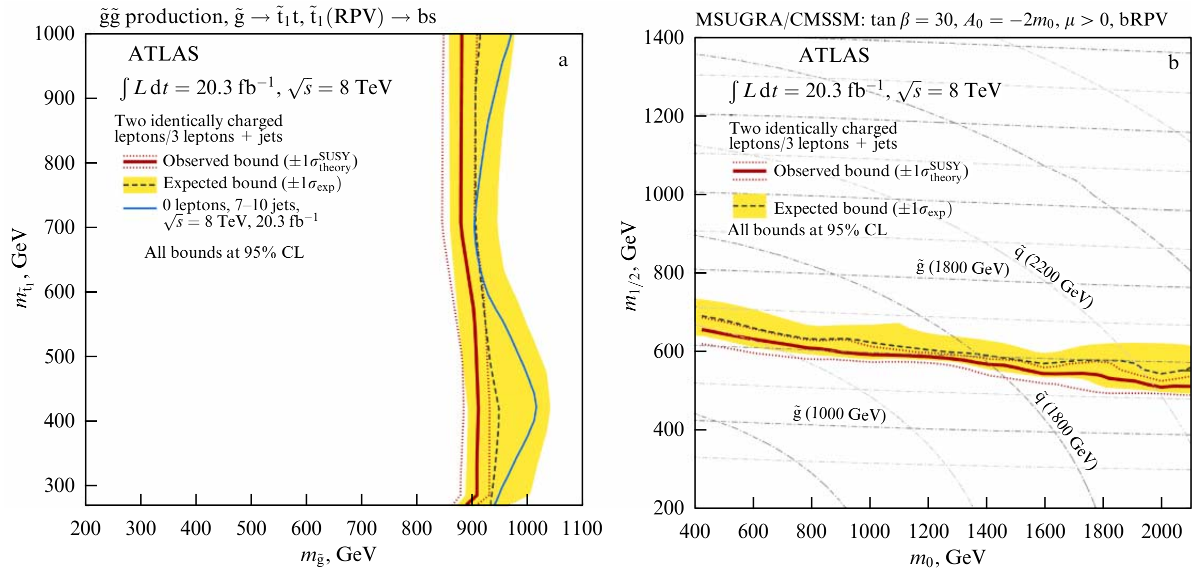

Figure 20. (Color online.) (a) Observed and expected contours of excluded gluino $\tilde{g}$ and $\tilde{t}_1$ masses. (b) Observed and expected contours of excluded values of m_0 and $m_{1/2}$ mass parameters in the bilinear RPV model obtained at $\sqrt{s} = 8$ TeV and integrated luminosity 20.3 fb^{-1} at a 95% confidence level [112]. Results of the previous analysis [106] are also shown.

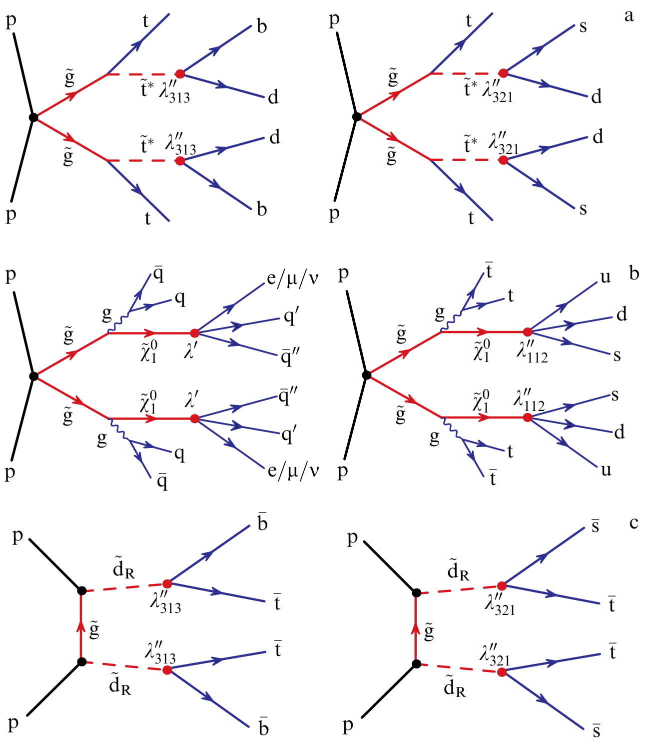

Figure 21. (Color online.) Feynman diagrams for RPV SUSY models of (a, b) gluino pair production and (c) t-channel production of a pair of right-handed squarks decaying with the respective baryon and lepton number violating constants λ'' and λ' ($q \equiv \mathrm{u, d, c, s}$).

The contributions of all background processes were estimated using Monte Carlo generators, except for the ones involving secondary leptons from decays of SM particles or processes with a photon conversion and erroneously reconstructed leptons, for example, from jets, which were determined from data based on the fact that all leptons have a probability of being reconstructed either as signal, ε, or as background, ζ.

From simulation of the $\mathrm{t\bar{t}}$-pair production processes, ε was determined as a function of p_{T} and η of the lepton. The value of ζ was determined from data in which a kinematic region with a large fraction of erroneously reconstructed leptons during $\mathrm{t\bar{t}}$-pair production was selected: two or three equally charged leptons, at least one b-jet, $E_{\mathrm{T}}^{\mathrm{miss}} > 30$ GeV, and no fewer than 2 to 3 jets.

As can be seen from Fig. 23, this analysis allowed excluding gluino masses below 1600 GeV for a $\tilde{t}$-squark mass below 1400 GeV at a 95% confidence level for a scenario in which the gluino decays successively into three tbs quarks or three tbd quarks.

A similar analysis was carried out by the CMS collaboration at $\sqrt{s} = 13$ TeV and the integrated luminosity of 35.9 fb^{-1} in searching for second-generation sleptons ($\tilde{\mu}_{\mathrm{L}}$, $\tilde{\nu}_{\mu}$) with two identically charged muons and at least two jets in the final state [116]. Only two scenarios of single slepton production with $\lambda'_{211} \neq 0$ were considered.

The first is charged slepton production

$$\mathrm{\bar{u}d} \to \tilde{\mu}_{\mathrm{L}}^- \to \tilde{\chi}_1^0 \mu^- \to \mu^- \tilde{\mu}_{\mathrm{L}}^{+*} \mu^- \to \mu^- \mathrm{u\bar{d}}\, \mu^- ,$$

and the second is the sneutrino production

$$\mathrm{d\bar{d}} \to \tilde{\nu}_{\mu} \to \tilde{\chi}_1^+ \mu^- \to \tilde{\chi}_1^0\, \mathrm{W}^+ \mu^-$$
$$\to \mu^- \tilde{\mu}_{\mathrm{L}}^{+*} \mathrm{q\bar{q}}' \mu^- \to \mu^- \mathrm{u\bar{d}q\bar{q}}' \mu^- .$$

The upper bounds for the cross sections of such processes, ranging from 0.00024 to 4.8 pb, were established at a 95% confidence level. In addition, the cross section bounds were recalculated to the bounds for the λ'_{211} coupling constant in the CMSSM with fixed parameters $\tan\beta = 20$, $A_0 = 0$, and $\mu > 0$, and the m_0 and $m_{1/2}$ parameters varied within the respective ranges of 300–3000 GeV and 300–3300 GeV. The obtained bounds for the λ'_{211} coupling constant ranged from 0.001 to 0.1, depending on the values of m_0 and $m_{1/2}$ [116].

Events with the final-state signature considered in this section correspond not only to the RPV constants mentioned in Section 5 but also to the violating constants such as λ'_{21k}, which can be calculated from the constraint on the process

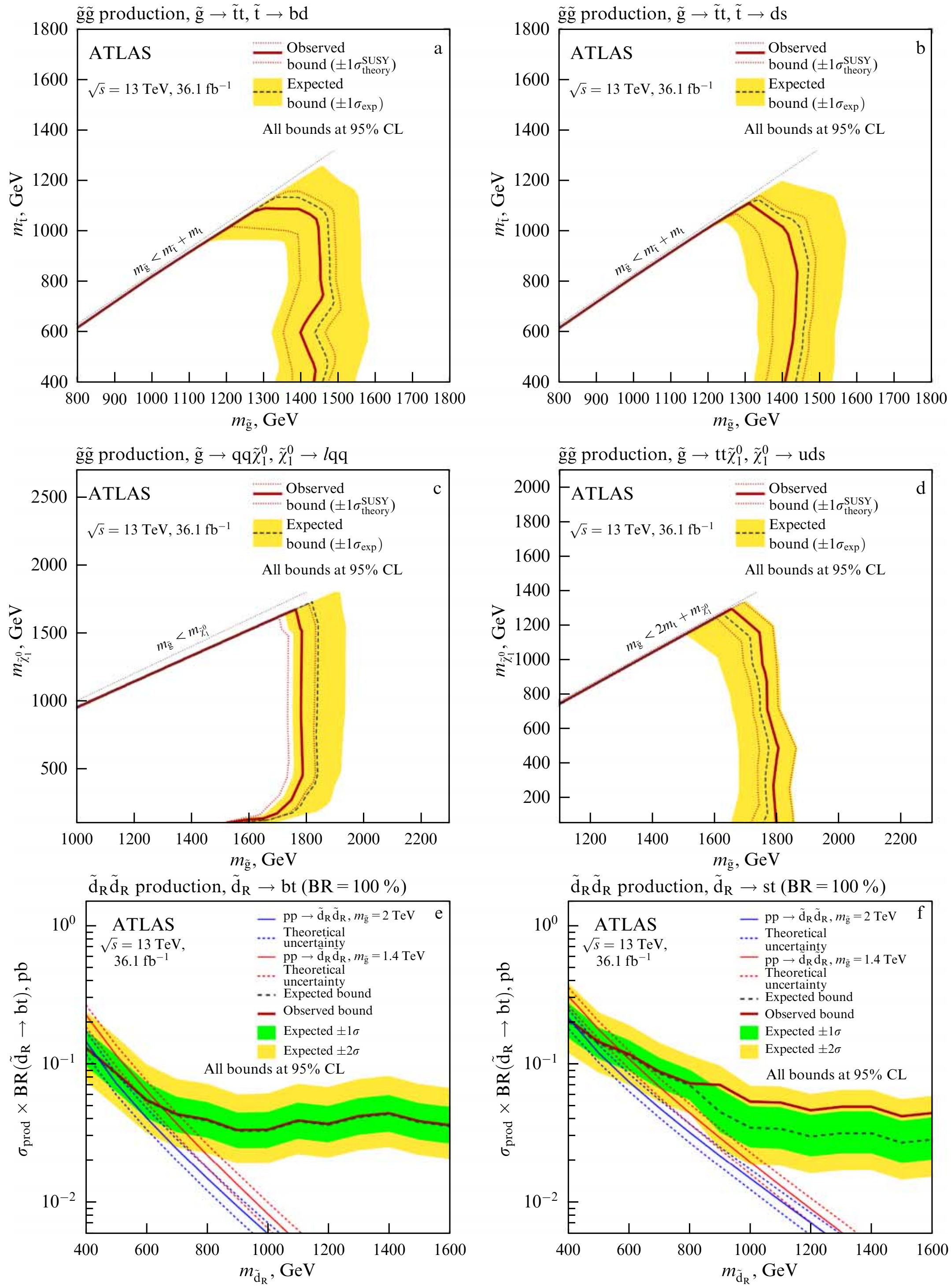

Figure 22. (Color online.) Observed and expected contours of the excluded (95% confidence level) $\tilde{g}$, $\tilde{t}$, $\tilde{d}_R$, and $\tilde{\chi}_1^0$ masses in 'simplified' RPV SUSY models due to the production of (a–d) only $\tilde{g}\tilde{g}$ pairs or (e, f) $\tilde{d}_R\tilde{d}_R$ with exclusive decay channels. For the $\pm 1\sigma$ error of the expected bound shown with a strip, the theoretical error was not taken into account. Dotted lines show changes in the observed bound with an increase or decrease in the theoretical signal production cross section within the theoretical error. Diagonal lines show the kinematic bound for a given decay channel [114].

universality violation due to charged currents and the ratio of the leptonic decay widths $\Gamma(\pi \to e\nu)/\Gamma(\pi \to \mu\nu)$ of the pion [82]:

$$\lambda'_{21k} < 0.02\,\frac{m_{\tilde{d}_{Rk}}}{M_W}\ \ (\text{ATLAS})\,.$$

The upper bound for the λ'_{21k} coupling constant for a squark mass of 1 TeV (2 TeV) hence follows as $\lambda'_{21k} < 0.25$ (< 0.50).

7. *R*-parity violation and third-generation squarks

Searches for third-generation squarks are often classified into a separate group of studies, because one consequence of the 'natural' SUSY scenario is that, due to large quantum corrections to the Higgs boson mass from top-quark loops, the stop quark $\tilde{t}$ and the sbottom quark $\tilde{b}$, being SUSY

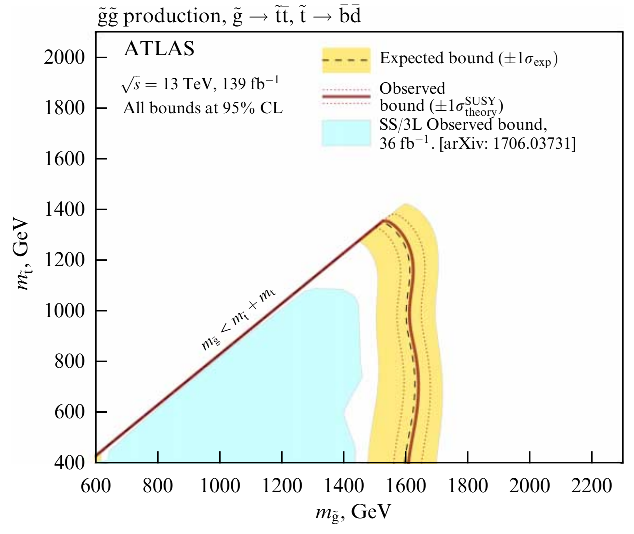

Figure 23. (Color online.) Observed and expected contours of excluded $\tilde{g}$ and $\tilde{t}$ masses in 'simplified' RPV SUSY models with only $\tilde{g}\tilde{g}$ pair production and exclusive decays $\tilde{g} \to \tilde{t}(\to \bar{b}\bar{d}/\bar{b}\bar{s})\bar{t}$ at a 95% confidence level [115]. For the $\pm 1\sigma$ error of the expected bound shown with a strip, the theoretical error of the cross section was not taken into account. Results of the previous analysis [114] are also shown.

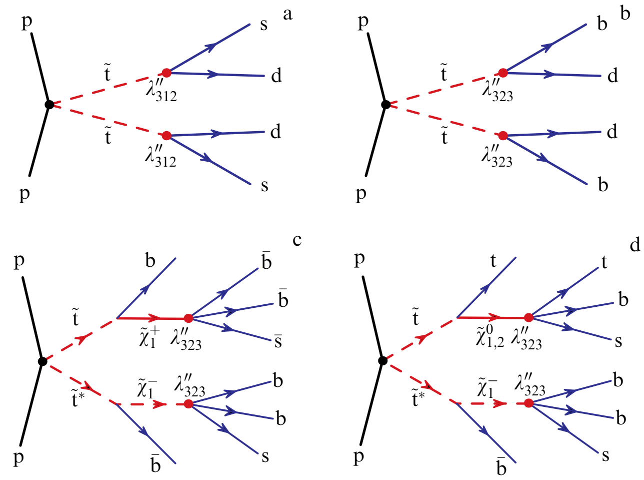

Figure 24. (Color online.) Production of a $\tilde{t}$-squark pair in the strong interaction with an RPV decay into (a) d and s quarks, (b) b and s quarks via nonzero λ'' constants, (c) a b quark and the lightest chargino $\tilde{\chi}_1^+$ ($\tilde{t} \to b\tilde{\chi}_1^+$) followed by chargino decay $\tilde{\chi}_1^+ \to \bar{b}\bar{b}\bar{s}$, and (d) a top quark and one of the two lightest neutralinos $\tilde{\chi}^0_{1,2}$ followed by $\tilde{\chi}^0_{1,2} \to$ tbs decay.

partners of third-generation SM quarks, can be relatively light (lighter than the superpartners of the quarks of the first two generations), not exceeding the scale of 1 TeV [3, 117].

Events with this signature in the final state can be caused by processes with the violating constants λ''_{3jk} or λ_{122} respectively described in Sections 5 and 4. In addition, a significant role is also played in such events by the λ_{233} violating constant, which can be calculated from the constraint on the universality of the coupling constants of quarks and leptons to the W boson [81, 82],

$$\lambda_{23k} < 0.03\,\frac{m_{\tilde{e}_{Rk}}}{M_W}\,.$$

The upper bounds for λ'_{233}, similarly to the λ''_{3jk} bounds, can be calculated in terms of corrections to the Z-boson decay into a pair of muons [102, 103]:

$$\lambda'_{233} < 1.03\,\frac{m_{\tilde{q}_{Rk}}}{M_W}\,.$$

This possibility was first analyzed experimentally by the ATLAS collaboration at $\sqrt{s} = 8$ TeV and the integrated luminosity 17.4 fb^{-1} [110]. The RPC process pp $\to \tilde{t}\tilde{t}^*$ was supposed to produce a $\tilde{t}\tilde{t}^*$ pair (an LSP pair) in which each $\tilde{t}$ squark decays due to the RPV constant λ''_{321} only into a $\bar{b}\bar{s}$-quark pair (Fig. 24b).

Because the masses of stop quarks were considered in the range of 100–400 GeV, a rough estimate of the collimation of the decay products of each of the stop quarks

$$\Delta R \approx 2\,\frac{m_{\tilde{t}}}{p_T}$$

showed that a $\bar{b}\bar{s}$ pair forms with a high probability one large jet (with $R \approx 1.5$). The variables used to suppress the background and to estimate its magnitude included the mass asymmetry of large jets

$$\mathcal{A} = \frac{|m_1 - m_2|}{m_1 + m_2}\,,$$

with $\mathcal{A} < 0.1$ in the SR, the number of b-jets (with $N_b \geqslant 2$ in the SR), the ratio of p_T for the a- and b-subjets inside each large jet,

$$p_T^{J_1,J_2} = \frac{\min\,[p_T(a), p_T(b)]}{\max\,[p_T(a), p_T(b)]}\,,$$

with $p_T^{J_1,J_2} > 0.3$ in the SR, and the escape angle of the produced pair of stop quarks relative to the beam axis determined in the center of mass system (with $|\cos\theta^*| < 0.3$ in the SR).

As in the analyses described above, the background was estimated using the distributions over the arithmetic mean mass of two large jets from the control regions, with at least one inverted selection criterion.

As can be seen in Fig. 25a, the production of a $\tilde{t}$-squark pair is ruled out at a 95% confidence level for masses from 100 to 315 GeV.

This analysis was subsequently extended to $\sqrt{s} = 13$ TeV and the integrated luminosity of 36.1 fb^{-1} [119] by including the $\tilde{t}$-squark decay channel into a pair of light quarks (Fig. 24a). Accordingly, one more SR without a criterion for the presence of b-jets in an event was added. The main background from multijet processes in this additional region was predicted by the ABCD method with the inversion of $\mathcal{A}$ and $|\cos\theta^*|$. As can be seen from Fig. 25, for the decay channel $\tilde{t} \to qq'$, the regions $100 < m_{\tilde{t}} < 410$ GeV (Fig. 25b) and $480 < m_{\tilde{t}} < 610$ GeV (Fig. 25c) for the $\tilde{t} \to$ bs decay channel are excluded at a 95% confidence level.

In Section 5, we mentioned the analysis of multijet events, which was extended by an additional criterion for the presence of a lepton (e or μ) in an event at $\sqrt{s} = 13$ TeV and the integrated luminosity of 36.1 fb^{-1} [109]. In addition to the processes of direct production of a pair of gluinos, this analysis also involved the process of direct production of a pair of $\tilde{t}\tilde{t}^*$ squarks with their subsequent decay into unstable charginos, $\tilde{\chi}_1^{\pm}$, and neutralinos, $\tilde{\chi}^0_{1,2}$ (Fig. 24c, d):

$$\tilde{t} \to t\tilde{\chi}^0_{1,2} \to \text{ttbs}\,, \quad \tilde{t}^* \to b\tilde{\chi}_1^{\pm} \to \text{bbbs}\,.$$

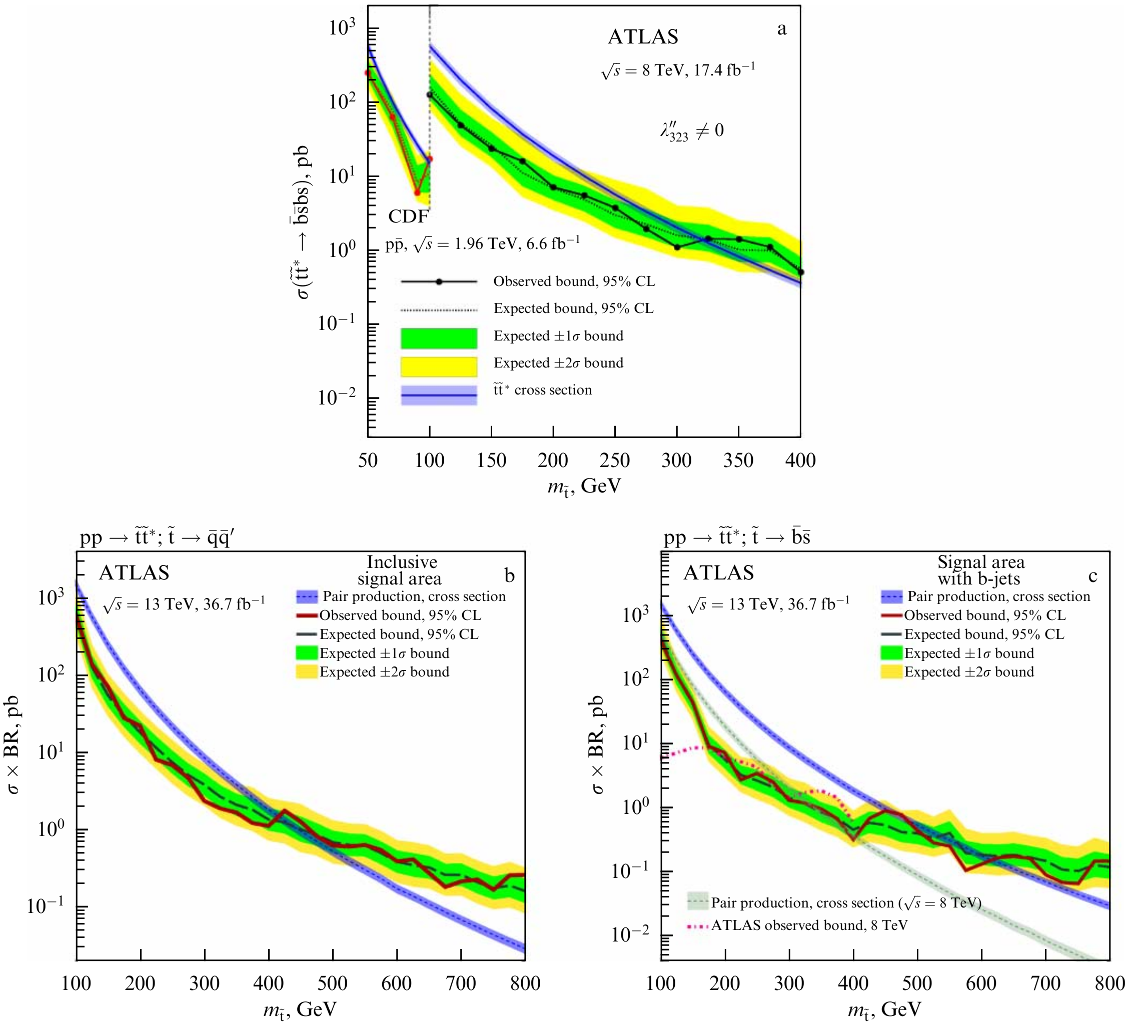

Figure 25. (Color online.) (a) Observed and expected upper bounds for the cross section for $\tilde{t}$-squark pair production as functions of the $\tilde{t}$-squark mass at a 95% confidence level. Black solid curve shows observed bounds, black dashed curve is the expected bound. Green and yellow bands show 1σ and 2σ errors of the expected bound. Also shown are results obtained by the CDF (Collider Detector at Fermilab) collaboration at the Tevatron accelerator [118] for $m_{\tilde{t}} \leqslant 100$ GeV [110]. Upper bound is shown at a 95% confidence level for the $\sigma \times$ Br value compared to theoretical predictions for direct $\tilde{t}$-squark pair production with (b) $\tilde{t} \to qq'$ and (c) $\tilde{t} \to \bar{b}\bar{s}$ decay channels. Expected and observed bounds are shown by dotted black and solid red curves, with all errors except the theoretical one for the signal production cross section taken into account. Green (yellow) areas show $\pm 1\sigma$ ($\pm 2\sigma$) deviations of the expected bound [119].

As a result, the mass bound for the $\tilde{t}$ squark was increased by a factor of 3–4, to 1.1 and 1.25 TeV for the respective higgsino and bino regarded as the LSP (Fig. 26a).

Similar final states of a squark pair $\tilde{t}\,\tilde{t}^*$ were considered in the next version of the analysis already at the integrated luminosity of 36.1 fb^{-1}, with the difference being that the t quarks decayed into hadrons [120]. Accordingly, events with at least one electron or muon were tossed out. In eight SRs, there must be $N_{\mathrm{j}} = 6, 7, 8$, and $\geqslant 9$ jets with $p_{\mathrm{T}} > 25$ GeV, and, for each N_{j}, the number of b-jets varied in the range from $N_{\mathrm{b}} = 4$ or $N_{\mathrm{b}} \geqslant 5$.

The main background process for the production of multijet events was estimated using the extrapolation of the probability ε to reconstruct the jet as a b-jet, depending on $p_{\mathrm{T}}/H_{\mathrm{T}}$, where H_{T} is the scalar sum over p_{T} of all jets in event (11), and $\Delta R_{\min}$ is the minimum distance in the $\eta - \phi$ plane between each jet and two to three jets with the maximum ε. Extrapolation was carried out in the control region with $N_{\mathrm{j}} = 5$ and $N_{\mathrm{b}} \geqslant 2$ for the b-jet multiplicity distribution for each value of N_{j} of SRs using the data with all other background events subtracted, such as single t-quark production, and the $\mathrm{t}\bar{\mathrm{t}}$ + jets/V/H processes derived from SM predictions. Models with the decay of both $\tilde{t}$ squarks into $\mathrm{b}\tilde{\chi}_1^{\pm}$ were also used for interpretation, and, for the model with $\tilde{\chi}^0_{1,2}$, bounds were only imposed for the dependence of the $\tilde{t}$ squark mass on the higgsino LSP mass (Fig. 26c and b). In both decay scenarios, $\tilde{t}$-squark masses less than 950 GeV were excluded.

In addition, at the same integrated luminosity and beam energy, lepton number violation was sought under the assumption that pp collisions produce only pairs of $\tilde{t}$ squarks, each of which decays into a charged lepton (an electron or a muon) and a b-quark [121].

This analysis is distinguished first and foremost by its relative simplicity due to the simplicity of the $\tilde{t} \to \mathrm{e}(\mu) + \mathrm{b}$ event signature. The probability amplitude of this RPV decay is proportional to the coupling constant $\lambda'_{31(2)3}$.

Two SRs of small and large masses of the $\tilde{t}$ squark were identified. The desired events were selected by the requirement that they contain at least one b-quark in order for the scalar sum (11) of the lepton and b-jet p_{T} to be $H_{\mathrm{T}} > 1$ TeV, for the largest invariant mass of the b-jet and the lepton to

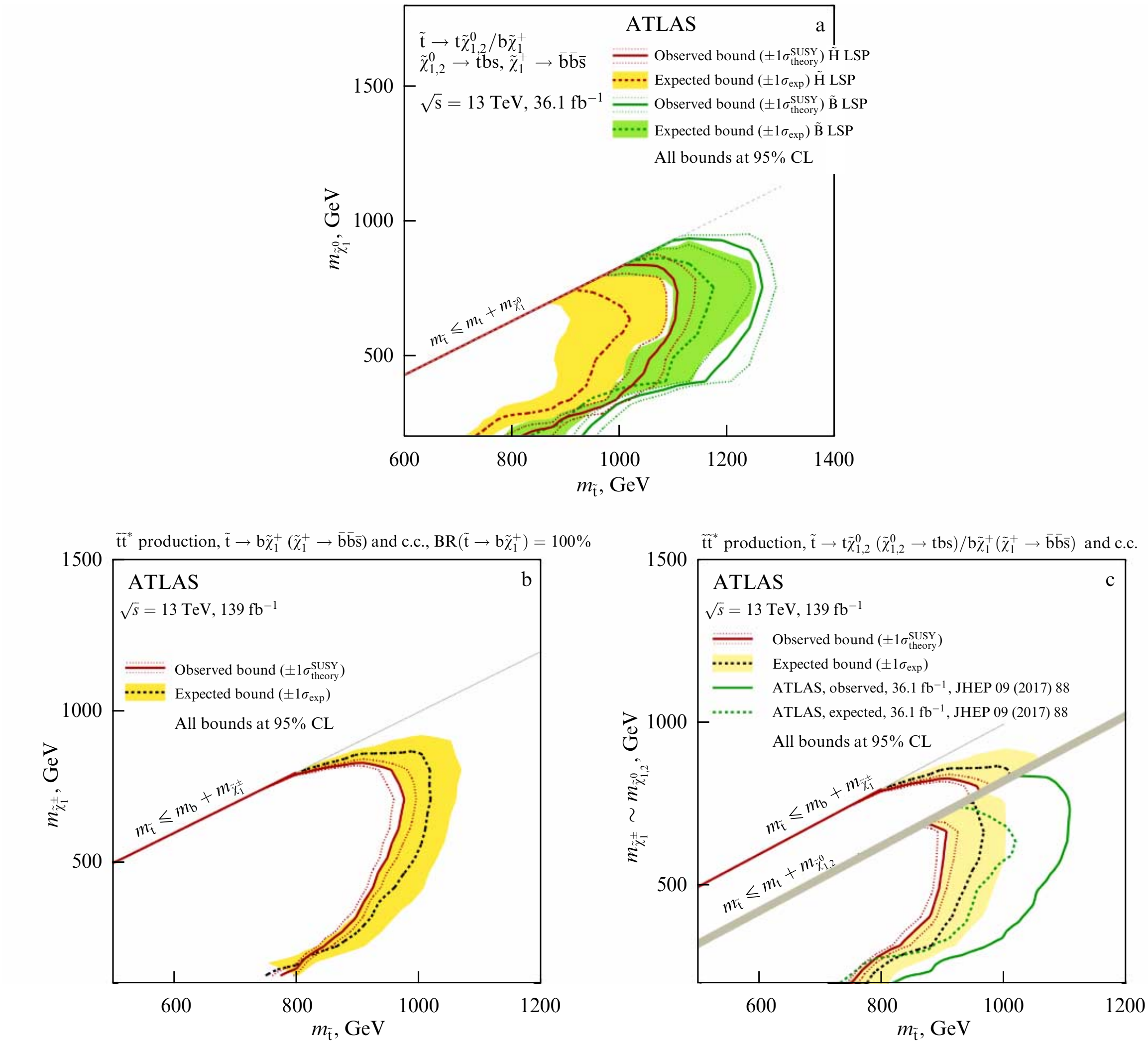

Figure 26. (Color online.) (a) Observed and expected contours of excluded $\tilde{t}$ and $\tilde{\chi}^0_1$ masses for the LSP represented by (b) a bino ($\tilde{B}$) and a higgsino ($\tilde{H}$), $\tilde{\chi}^\pm_1$ and (c) a higgsino $\tilde{\chi}^\pm_1$ for direct $\tilde{t}$-squark pair production within the RPV scenario and an unstable LSP. For the $\pm 1\sigma$ error of the expected bound shown with a strip, the theoretical error of the signal production cross section was not taken into account. Dotted curves show changes in the observed bound with an increase or decrease in the theoretical cross section for signal production within the theoretical error. All bounds were obtained at a 95% confidence level. Diagonal lines show the kinematic bound for a given decay channel [109, 120].

be greater than 800/1100 GeV and for their smallest invariant mass to exceed 150 GeV, and for the invariant mass of a pair of leptons to exceed 300 GeV. These criteria allowed significantly suppressing the main background from the processes of direct production of a pair of $t\bar{t}$ quarks, single t-quark production, and the formation of Z + jets.

To estimate the magnitude of each of these background processes, a control region was used in which the dominance of the corresponding background was ensured by inverting several SR selection criteria. The shapes of the background distributions were not taken into account in any way, and their normalization coefficients were extrapolated based only on the statistics obtained from SM predictions, while other insignificant background processes, such as W + jets, production of a pair of vector bosons, and $t\bar{t}$ + W/Z, were taken into account based only on SM predictions.

The bounds for the cross section of a production of a pair of $\tilde{t}$ squarks were calculated depending on the probability of the RPV decay of one stop quark into e, μ, or τ. The sum of these probabilities was normalized to unity.

As can be seen from Fig. 27, at large ($\geqslant 0.7$) values of the $\tilde{t}$-squark decay probability into a τ lepton, only small $\tilde{t}$-squark masses, from 600 to 1000 GeV, were excluded, whereas the $\tilde{t}$-squark masses above 1000 GeV can be excluded in this model only if the probability of $\tilde{t}$-squark decay into a τ lepton is less than 0.5.

The best mass bound for the $\tilde{t}$ squark obtained by the CMS collaboration was established by studying events with 3 to 4 charged leptons (e, μ, and τ) in the final state at $\sqrt{s} = 8$ TeV and an integrated luminosity of 19.5 fb^{-1} [122].

Considered in this analysis was the decay of a produced $\tilde{t}$-squark pair via $\tilde{t} \to \tilde{\chi}^{0*}_1 t$ followed by the decay of the neutralino via the lepton channel, $\tilde{\chi}^{0*}_1 \to l_i \nu_j l_k$ and $\tilde{\chi}^{0*}_1 \to \nu_i l_j l_k$, with nonzero respective coupling constants λ_{122} and λ_{233}. The semileptonic neutralino decay channel $\tilde{\chi}^{0*}_1 \to \mu t \bar{b}/\nu b \bar{b}$ with $\lambda'_{233} \neq 0$ was also considered. The observed bound was 1080 GeV for $\lambda_{122} \neq 0$ and 900 GeV for $\lambda_{233} \neq 0$ in the neutralino mass range of 100–1300 GeV at a 95% confidence level. Using the same data, a search was made for direct $\tilde{b}$-squark pair production with the squark decay $\tilde{b} \to \bar{t}\bar{s}/\bar{d}$ for $\lambda''_{332}/\lambda''_{331} \neq 0$, followed by a leptonic

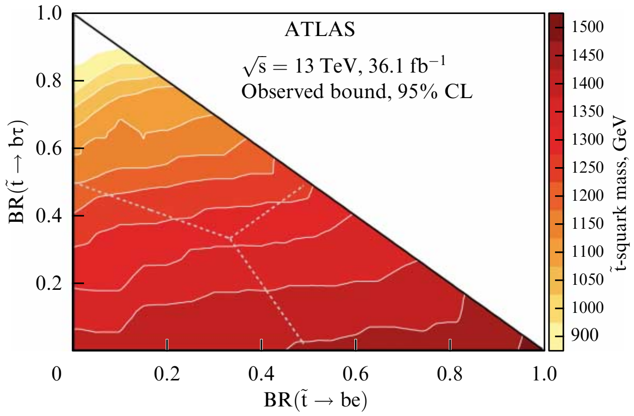

Figure 27. (Color online.) Observable bounds of the $\tilde{t}$-squark pair production cross section for various $\tilde{t}$-squark masses as functions of the decay branching into e or τ at a 95% confidence level [121].

decay of both top quarks. The mass bound for the $\tilde{b}$ squark was found to be 307 GeV at a 95% confidence level [101].

Estimates for the upper bounds of violating constants such as λ''_{3jk}, λ_{122}, or λ_{23k} are discussed in Sections 3–6. However, the upper bound for the λ'_{233} violating constant can be calculated assuming that the $\tilde{t}$-squark mass is 1080 GeV. Hence, the bound for λ'_{233} is $\lambda'_{233} < 13.8$.

8. Conclusion

We have presented the results of all the work done by the ATLAS collaboration on the search for possible manifestations of SUSY with broken R-parity in the data obtained in 2009–2018. At the same time, the development of methods for selecting signal events and estimating the contribution of background processes was discussed in detail.

In Section 3, we analyzed the results of the search by the ATLAS collaboration for manifestations of RPV effects both in the production of SUSY particles and in their decays. The probability amplitudes of such processes are proportional to the products of at least two RPV coupling constants of the $\lambda'\lambda''$ type. Experimental bounds are imposed on combinations of RPV constants in the form $f_{d\bar{d}}|\lambda'_{131}\lambda'_{231}|^2 + f_{s\bar{s}}|\lambda'_{132}\lambda'_{232}|^2$ and on the RPV coupling constant λ'_{311} depending on the tau-sneutrino mass and various assumptions about the λ_{i3k} coupling constants for eμ, eτ, and $\mu\tau$.

In Section 4, we considered RPV SUSY processes whose amplitudes are proportional to a single coupling constant λ from the lepton sector. In Section 5, we discussed the RPC processes of production of gluino or squark pairs, which, when decaying into SM quarks, produce multijet events in the final state due to RPV λ'' coupling constants in the hadron sector. The extension of this study to the case of multijet events accompanied by two identically charged leptons or three leptons was discussed in Section 6. The extended study is potentially sensitive not only to RPV λ'' hadron coupling constants but also to RPV constants λ' that mix the lepton and hadron sectors. Phenomenologically, these constants can be considered effective constants of the lepton–quark interaction.

The processes of both the electroweak production of SUSY particles, chargino or neutralino, and the production of gluinos and squarks due to the strong interaction have been discussed. Special attention was directed in Section 7 to RPV decays of rather light (at the 1 TeV scale) superpartners of top quarks, the $\tilde{t}$ squarks.

In general, the studies discussed in this review of the possibility of detecting SUSY particles from their RPV decay channels allowed the ATLAS collaboration to improve the lower mass bounds for supersymmetric particles by about 2 to 3 times. For example, the best values are 1050 GeV for sleptons and sneutrinos, 1400 GeV for charginos and neutralinos, 2100 GeV for gluinos, and 1000 GeV for the $\tilde{t}$ quark. The corresponding lower bounds obtained in the CMS experiment were 1280 (2800) GeV for a slepton, depending on the RPV constants λ_{132}, λ_{231}, and λ'_{311}, 1610 GeV for the gluino, and 1080 GeV for the $\tilde{t}$ quark [80, 122, 123]. In addition, constraints on the fundamental coupling constants from the RPV superpotential have been obtained. Their upper bounds are also given based on other experimental data.

These 'collider R-parity constraints,' which correspond to the maximum collision energy, are of undoubted interest from the standpoint of the search for New Physics in 'low-energy' processes, such as rare decays of elementary particles (see, e.g., [27, 36, 58, 124]) or neutrino phenomena (see, e.g., [29, 32, 34, 125, 126]).

We note that the lower bounds for the masses of SUSY particles mentioned above cannot be called model independent, strictly speaking. They are almost always obtained within the framework of a specific assumption both about the production process and about the types of decay of these SUSY particles.

Unfortunately, nothing better can be offered at the present time, for the simple reason that none of the studies carried out in almost 10 years by the ATLAS and CMS collaborations at the LHC yielded any significant indications, for example, as to the phenomena with the missing momentum values $E_{\mathrm{T}}^{\mathrm{miss}}$ that could not be satisfactorily described within the current SM.

In other words, we currently have no experimental hints of New Physics, the most striking and most expected manifestation of which at the LHC was considered to be the energy imbalance expressed in the large values of $E_{\mathrm{T}}^{\mathrm{miss}}$, inexplicable from the SM standpoint. In SUSY models, as is known, the source of such a large missing momentum is usually assumed to be the lightest massive, stable, and weakly interacting LSP.

This justifies attempts to search for SUSY particles based on the assumption of their RPV channels, because these decays naturally (without a stable LSP) form the final states of high-energy pp interactions, not different in any way from the final states expected in the SM framework.

Hence, in the absence of any significant indications as to the existence of physics beyond the SM in LHC experiments, the search for New Physics 'embodied' by SUSY with RPV becomes especially important. A possible way to further develop this field can therefore be the analysis of SUSY phenomena that took place under the RPC assumption, now without requiring the presence of a large $E_{\mathrm{T}}^{\mathrm{miss}}$ in the event caused by an unregistered stable LSP. Preliminary estimates carried out, for example, in [58] showed that this approach is promising, at least for processes with $\lambda_{ijk} \neq 0$ at energy $\sqrt{s} = 8$ TeV.

References

1. Aad G et al. (ATLAS Collab.) *Phys. Lett. B* **716** 1 (2012)
2. Chatrchyan S et al. (CMS Collab.) *Phys. Lett. B* **716** 30 (2012)

3. Barbieri R, Giudice G F *Nucl. Phys. B* **306** 63 (1988)
4. de Carlos B, Casas J A *Phys. Lett. B* **309** 320 (1993)
5. Bertone G, Hooper D, Silk J *Phys. Rep.* **405** 279 (2005)
6. Fayet P *Nucl. Phys. B Proc. Suppl.* **101** 81 (2001)
7. Quigg C, in *2nd CERN-CLAF School of High Energy Physics, 1–14 June 2003, San Miguel Regla, Mexico*, p. 57; hep-ph/0404228
8. Csáki C, Tanedo P, in *Proc. of the 2013 European School of High-Energy Physics, Parádfürdó, Hungary, 5–18 June 2013* Vol. 4 (CERN-2015-004, Eds M Mulders, G Perez) Vol. 4 (Geneva: CERN, 2015) p. 169, https://doi.org/10.5170/CERN-2015-004.169
9. Ross G G, in *Proc. of the 11th Intern. Conf. on Neutrino Physics and Astrophysics, 11–16 June, 1984, Nordkirchen near Dortmund* (Eds K Kleinknecht, E A Paschos, H Yuta) (Singapore: World Scientific, 1984) p. 606
10. Mohapatra R N *Unification and Supersymmetry: the Frontiers of Quark-Lepton Physics* (Berlin: Springer, 1986)
11. Nath P *Eur. Phys. J. Spec. Top.* **229** 3047 (2020)
12. Nath P *Supersymmetry, Supergravity, and Unification* (Cambridge: Cambridge Univ. Press, 2017)
13. Tata X *Eur. Phys. J. Spec. Top.* **229** 3061 (2020)
14. Bento M C, Hall L, Ross G G *Nucl. Phys. B* **292** 400 (1987)
15. Giudice G F, Rattazzi R, Wells J D *Nucl. Phys. B* **544** 3 (1999)
16. Golfand Y A, Likhtman E P *JETP Lett.* **13** 323 (1971); *Pis'ma Zh. Eksp. Teor. Fiz.* **13** 452 (1971)
17. Volkov D V, Akulov V P *Phys. Lett. B* **46** 109 (1973)
18. Wess J, Zumino B *Nucl. Phys. B* **70** 39 (1974)
19. Wess J, Zumino B *Nucl. Phys. B* **78** 1 (1974)
20. Ferrara S, Zumino B *Nucl. Phys. B* **79** 413 (1974)
21. Salam A, Strathdee J *Phys. Lett. B* **51** 353 (1974)
22. Sakai N *Z. Phys. C* **11** 153 (1981)
23. Dimopoulos S, Raby S, Wilczek F *Phys. Rev. D* **24** 1681 (1981)
24. Ibáñez L E, Ross G G *Phys. Lett. B* **105** 439 (1981)
25. Dimopoulos S, Georgi H *Nucl. Phys. B* **193** 150 (1981)
26. Inoue K et al. *Prog. Theor. Phys.* **68** 927 (1982); *Prog. Theor. Phys.* **70** 330 (1983) Errata
27. Ellis J, Rudaz S *Phys. Lett. B* **128** 248 (1983)
28. Farrar G R, Fayet P *Phys. Lett. B* **76** 575 (1978)
29. Mitsou V A *PoS* **258** 085 (2015)
30. Hall L J, Suzuki M *Nucl. Phys. B* **231** 419 (1984)
31. Banks T et al. *Phys. Rev. D* **52** 5319 (1995)
32. Nilles H-P, Polonsky N *Nucl. Phys. B* **484** 33 (1997)
33. Nardi E *Phys. Rev. D* **55** 5772 (1997)
34. Borzumati F M et al. *Phys. Lett. B* **384** 123 (1996)
35. Dimopoulos S, Raby S, Wilczek F *Phys. Lett. B* **112** 133 (1982)
36. Sakai N, Yanagida T *Nucl. Phys. B* **197** 533 (1982)
37. Weinberg S *Phys. Rev. D* **26** 287 (1982)
38. Zyla P A et al. (Particle Data Group) *Prog. Theor. Exp. Phys.* **2020** 083C01 (2020)
39. Giudice G F, Rattazzi R *Phys. Lett. B* **406** 321 (1997)
40. Brahm D E, Hall L J *Phys. Rev. D* **40** 2449 (1989)
41. Tamvakis K *Phys. Lett. B* **382** 251 (1996)
42. Quevedo F, Krippendorf S, Schlotterer O "Cambridge lectures on supersymmetry and extra dimensions", arXiv:1011.1491
43. Kuriyama M, Nakajima H, Watari T *Phys. Rev. D* **79** 075002 (2009)
44. Kim J E *Phys. Rev. D* **104** 016012 (2021)
45. Bednyakov V A *Phys. Part. Nucl.* **44** 220 (2013); *Fiz. Elem. Chastits At. Yadra* **44** 429 (2013)
46. Bednyakov V A *Phys. Part. Nucl.* **47** 711 (2016); *Fiz. Elem. Chastits At. Yadra* **47** 1314 (2016)
47. Aaltonen T et al. (CDF Collab.) *Phys. Rev. Lett.* **105** 191801 (2010)
48. CDF Collab., Public Note CDF 7835, unpublished
49. CDF Collab., CDF Conference Note 8228, unpublished (2006)
50. Abbott B et al. (D0 Collab.) *Phys. Rev. Lett.* **83** 4476 (1999)
51. Abbott B et al. (D0 Collab.) *Phys. Rev. D* **62** 071701 (2000)
52. Abazov V M et al. (D0 Collab.) *Phys. Rev. Lett.* **89** 171801 (2002)
53. Abazov V M et al. (D0 Collab.) *Phys. Rev. Lett.* **89** 261801 (2002)
54. Abazov V M et al. (D0 Collab.) *Phys. Lett. B* **638** 441 (2006)
55. Abazov V M et al. (D0 Collab.) *Phys. Rev. Lett.* **97** 111801 (2006)
56. Abazov V M et al. (D0 Collab.) *Phys. Rev. Lett.* **100** 241803 (2008)
57. Abazov V M et al. (D0 Collab.) *Phys. Rev. Lett.* **105** 191802 (2010)
58. Dercks D et al. *Eur. Phys. J. C* **77** 856 (2017)
59. Barbier R et al. *Phys. Rep.* **420** 1 (2005)
60. Chemtob M *Prog. Part. Nucl. Phys.* **54** 71 (2005)
61. Allanach B C, Dedes A, Dreiner H K *Phys. Rev. D* **69** 115002 (2004); *Phys. Rev. D* **72** 079902 (2005) Erratum
62. ATLAS Experiment — Public Results. Public ATLAS Luminosity Results for Run-2 of the LHC , https://twiki.cern.ch/twiki/bin/view/AtlasPublic/LuminosityPublicResultsRun2
63. Aad G et al. (ATLAS Collab.) *JINST* **3** S08003 (2008)
64. Capeans M et al. (ATLAS Collab.) "ATLAS Insertable B-Layer technical design report", CERN-LHCC-2010-013, ATLAS Technical Design Report 19 (Geneva: CERN, 2010)
65. ATLAS Collab. "ATLAS Insertable B-Layer technical design report addendum", CERN-LHCC-2012-009, ATLAS Technical Design Report 19 ADD-1 (Geneva: CERN, 2012)
66. Abbott B et al. *JINST* **13** T05008 (2018)
67. Aaboud M et al. (ATLAS Collab.) *Eur. Phys. J. C* **77** 317 (2017)
68. Aad G et al. (ATLAS Collab.) *Phys. Rev. Lett.* **106** 251801 (2011)
69. Aad G et al. (ATLAS Collab.) *Eur. Phys. J. C* **71** 1809 (2011)
70. Shao-Ming W et al. *Phys. Rev. D* **74** 057902 (2006)
71. Shao-Ming W et al. *Chinese Phys. Lett.* **25** 58 (2008)
72. Agostinelli S et al. *Nucl. Instrum. Meth. Phys. Res. A* **506** 250 (2003)
73. Aad G et al. (ATLAS Collab.) *Eur. Phys. J. C* **72** 2040 (2012)
74. Chaichian M, Huitu K *Phys. Lett. B* **384** 157 (1996)
75. Huitu K et al. *Phys. Lett. B* **430** 355 (1998)
76. Aad G et al. (ATLAS Collab.) *Phys. Rev. Lett.* **115** 031801 (2015)
77. Aad G et al. (ATLAS Collab.) *Phys. Lett. B* **723** 15 (2013)
78. Aaboud M et al. (ATLAS Collab.) *Eur. Phys. J. C* **76** 541 (2016)
79. Aad G et al. (ATLAS Collab.) *Phys. Lett. B* **801** 135114 (2020)
80. Khachatryan V et al. *Eur. Phys. J. C* **76** (6) 317 (2016)
81. Dreiner H K, in *Perspectives on Supersymmetry II* (Advanced Ser. on Directions in High Energy Physics, Vol. 21, Ed. G L Kane) (Singapore: World Scientific, 2010) p. 565, https://doi.org/10.1142/9789814307505_0017
82. Barger V D, Giudice G F, Han T *Phys. Rev. D* **40** 2987 (1989)
83. Aulakh C S, Mohapatra R N *Phys. Lett. B* **119** 136 (1982)
84. Ross G G, Valle J W F *Phys. Lett. B* **151** 375 (1985)
85. Ellis J R et al. *Phys. Lett. B* **150** 142 (1985)
86. Santamaria A, Valle J W F *Phys. Lett. B* **195** 423 (1987)
87. Santamaria A, Valle J W F *Phys. Rev. Lett.* **60** 397 (1988)
88. Romão J C, Santos C A, Valle J W F *Phys. Lett. B* **288** 311 (1992)
89. Gonzalez-Garcia M C, Romão J C, Valle J W F *Nucl. Phys. B* **391** 100 (1993)
90. Barbieri R et al. *Phys. Lett. B* **238** 86 (1990)
91. Dimopoulos S, Hall L J *Phys. Lett. B* **207** 210 (1988)
92. Aad G et al. (ATLAS Collab.) *Phys. Rev. D* **90** 052001 (2014)
93. Aad G et al. (ATLAS Collab.) *J. High Energy Phys.* **2012** (12) 124 (2012)
94. Alwall J, Schuster P C, Toro N *Phys. Rev. D* **79** 075020 (2009)
95. Desch K et al. *Phys. Rev. D* **83** 015013 (2011)
96. Nakamura K (Particle Data Group) *J. Phys. G* **37** 075021 (2010)
97. Abazov V et al. (D0 Collab.) *Phys. Lett. B* **638** 441 (2006)
98. Beringer J et al. (Particle Data Group) *Phys. Rev. D* **86** 010001 (2012)
99. Aaboud M et al. (ATLAS Collab.) *Phys. Rev. D* **98** 032009 (2018)
100. Chatrchyan S et al. (CMS Collab.) *J. High Energy Phys.* **2012** (06) 169 (2012)
101. Khachatryan V et al. (CMS Collab.) *Phys. Rev. D* **94** 112009 (2016)
102. Ellis J R, Lola S, Sridhar K *Phys. Lett. B* **408** 252 (1997)
103. Bhattacharyya G, Choudhury D, Sridhar K *Phys. Lett. B* **355** 193 (1995)
104. Goity J L, Sher M *Phys. Lett. B* **346** 69 (1995); *Phys. Lett. B* **385** 500 (1996) Erratum
105. Aad G et al. (ATLAS Collab.) *J. High Energy Phys.* **2012** (12) 86 (2012)
106. Aad G et al. (ATLAS Collab.) *J. High Energy Phys.* **2013** (10) 130 (2013); *J. High Energy Phys.* **2014** (01) 109 (2014) Erratum
107. Aad G et al. (ATLAS Collab.) *Phys. Rev. D* **91** 112016 (2015)
108. Aaboud M et al. (ATLAS Collab.) *Phys. Lett. B* **785** 136 (2018)
109. Aaboud M et al. (ATLAS Collab.) *J. High Energy Phys.* **2017** (09) 88 (2017)
110. Aad G et al. (ATLAS Collab.) *J. High Energy Phys.* **2016** (06) 067 (2016)
111. Khachatryan V et al. (CMS Collab.) *Phys. Lett. B* **770** 257 (2017)
112. Aad G et al. (ATLAS Collab.) *J. High Energy Phys.* **2014** (06) 035 (2014)

113. Roy S, Mukhopadhyaya B *Phys. Rev. D* **55** 7020 (1997)
114. Aaboud M et al. (ATLAS Collab.) *J. High Energy Phys.* **2017** (09) 084 (2017); *J. High Energy Phys.* **2019** (08) 121 (2019) Erratum
115. Aad G et al. (ATLAS Collab.) *J. High Energy Phys.* **2020** (06) 046 (2020)
116. Sirunyan A M et al. (CMS Collab.) *Eur. Phys. J. C* **79** 305 (2019)
117. de Carlos B, Casas J A *Phys. Lett. B* **309** 320 (1993)
118. Aaltonen T et al. (CDF Collab.) *Phys. Rev. Lett.* **111** 031802 (2013)
119. Aaboud M et al. (ATLAS Collab.) *Eur. Phys. J. C* **78** 250 (2018)
120. Aad G et al. (ATLAS Collab.) *Eur. Phys. J. C* **81** (1) 11 (2021)
121. Aaboud M et al. (ATLAS Collab.) *Phys. Rev. D* **97** 032003 (2018)
122. Chatrchyan S et al. (CMS Collab.) *Phys. Rev. Lett.* **111** 221801 (2013)
123. Sirunyan A M et al. (CMS Collab.) *Phys. Lett. B* **783** 114 (2018)
124. Bednyakov V A *JINR Rapid Commun.* (1(93)-99) 30 (1999)
125. Allanach B C, Kom C H *J. High Energy Phys.* **2008** (04) 081 (2008)
126. Bednyakov V, Faessler A, Kovalenko S *Phys. Lett. B* **442** 203 (1998)